THESIS

DIAGENESIS, COMPOSITION AND POROSITY OF THE UPPER THREE FORKS FORMATION, WILLISTON BASIN, NORTH DAKOTA AND MONTANA

Submitted by

Ketki Kolte

Department of Geosciences

In partial fulfillment of the requirements

For the Degree of Master of Science

Colorado State University

Fort Collins, Colorado

Spring 2014

Master's Committee:

Advisor: Sven Egenhoff

Michael Ronayne
Mark Paschke

ABSTRACT

DIAGENESIS, COMPOSITION AND POROSITY OF THE UPPER THREE FORKS FORMATION, WILLISTON BASIN, NORTH DAKOTA AND MONTANA

The upper part of the Three Forks Formation in the Williston basin of North Dakota and Montana is one of the prime targets for oil exploration in the onshore part of the US today. The unit is mainly composed of dolomite, yet the details of dolomite formation and its relative timing are unknown. This study is the first that combines an analysis of cement generations and porosity to develop a diagenetic scheme based on detailed microscopical observations. The upper Three Forks Formation shows a total of seven dolomite generations along with some anhydrite and pyrite. Most of the rock consists of an inclusion-rich dolomite, likely dolomite II, that forms mm- to sub-mm-size rhombic crystals showing overgrowth of five more alternating clear and inclusion-rich dolomite generations, and in places a core of iron-rich dolomite I. Porosity types in the upper Three Forks Formation are intercrystalline, intracrystaline, and "moldic" which here stands for the dissolution of entire dolomite crystals. Detrital components are quartz, feldspars, mica, and clay particles.

The Three Forks Formation was most likely deposited on a mixed carbonate-siliciclastic ramp as a limestone unit with varying amounts of detrital input. Initial replacement of limestone into dolomite probably occurred early entirely changing the texture of this unit. Several dolomite phases occurred during burial post-dating early dolomitization. The effective porosity, characterized by intercrystalline and "moldic" pores, is linked to the dolomitization, most likely originally to an early event as no late dolomite is seen filing these pores. Up to centimeter-size voids, though, representing mostly non-effective porosity is generally partly filled with several

generations of dolomite and leaving some part of the vugs open. This indicates that most likely the voids were formed before the last few generations of dolomite cement, and also that not all open space was easily occluded by these dolomitizations but left some of the porosity untouched. Based on a limited data set, porosity distribution in the upper Three Forks Formation does not show a clear link to the distribution of dolomite. However, it does show a trend to overall increased values from the east (less than 1%) to the west (around 5%) with a north-south extending zone of maximum porosities (about 10-12%) around 103.5°. It is therefore likely that potential hot spots in this basin are rather located in western ND while towards the east porosities are lower.

ACKNOWLEDGMENTS

First, I would like to thank the Rocky Mountain Association of Geologists (RMAG) for supporting my research by awarding me Norman Foster's Scholarship in 2011 to carry out this project. Thank you to my advisor, mentor and guide, Dr. Sven Egenhoff for informing about this project and letting me be a part of it. I would also like to thank him for his support and contribution to this project. Thanks to Julie LeFever of North Dakota Geological Survey (NDGS) for helping us during our visits to Grand Forks, North Dakota. Thanks to Heather Lowers for assisting us with the Scanning Electron Microscope (SEM) and the microprobe at the United States Geological Survey (USGS), Denver. I would also like to thank Colorado State University (CSU) for rendering constant resources for fieldwork and also throughout the duration of my Master's degree. I would like to extend my sincerest thanks to my committee members, Dr. Michael Ronayne and Dr. Mark Paschke of CSU for their guidance and suggestions. Thank you also the former Heads of the Department (HOD), Dr. John Ridley and Dr. Sally Sutton, for allowing me to use the research microscope whenever needed. I would graciously like to thank every individual who came together in this project to give me technical guidance and moral support for this research. Also, I would like to extend my heartfelt thank you to all of the faculty and staff of CSU and University of Pune for providing me a very good foundation in geosciences. I would like to thank all my friends who have been extremely understanding throughout this journey. Thanks to Shashank for all the support he has given me throughout this time. I would finally like to thank my grandparents, parents, in-laws and the rest of my family for always giving me a helping hand whenever needed.

TABLE OF CONTENTS

CHAPTER 1: INTRODUCTION

The Williston basin is an elliptical intracratonic depression that contains numerous oil rich formations (Gerhard et al., 1990). Underlying the widely recognized Bakken Formation is the Three Forks Formation (Pitman et al., 2001). The Devonian Three Forks Formation, deposited approximately 390 million years ago is one of the productive reservoirs in the Williston basin of North Dakota and Montana (Nicolas, 2007). It has recently gained enormous importance for its oil potential (Beitsch, 2010). With increasing oil prices, it has become one of the substantially targeted formations in this region. The upper Three Forks Formation comprises mainly dolomitic rocks, making up the potential reservoir in this formation (Heck et al., 2002). The sequence stratigraphy and the depositional history of the Three Forks Formation have been previously explored by Egenhoff et al. (2011), but detailed compositional variations, diagenetic history and types of porosities of this formation have remained unclear to date. This study will therefore focus on unraveling the cement chronology, undefined and poorly understood mineralogical composition and establishing a porosity makeup for the dolomitic portion of the upper Three Forks Formation.

The main objectives of this study are (1) to identify the composition of crystals and grains in the cements and matrix of the dolomitic rock; (2) to describe the porosity types and reconstruct their formation and evolution during and after deposition, and (3) to develop a diagenetic model by identifying the timing of different generations of cements in the upper Three Forks Formation. This study also encompasses creating porosity and cement distribution maps that will enable delineation of potential “sweet spots” in areas where the porosities are highest, and reconstructing fluid flow prevalent during the diagenetic phase within the upper Three Forks Formation. These maps will in turn help in establishing ideal drilling locations where oil and gas

reserves are most likely to occur. This study is based on forty-two thin sections from sixteen cores, shown in Figure 1, collected from North Dakota Geological Survey (NDGS) in Grand Forks, ND and United States Geological Survey (USGS) in Denver, CO. Details for each core are provided in Appendix I – Table 1. Petrological microscope, scanning electron microscope (SEM) and electron microprobe observations along with point counting data, core digitizing, detailed descriptions will enable to understand and interpret the composition, porosity and diagenesis of the upper Three Forks Formation.

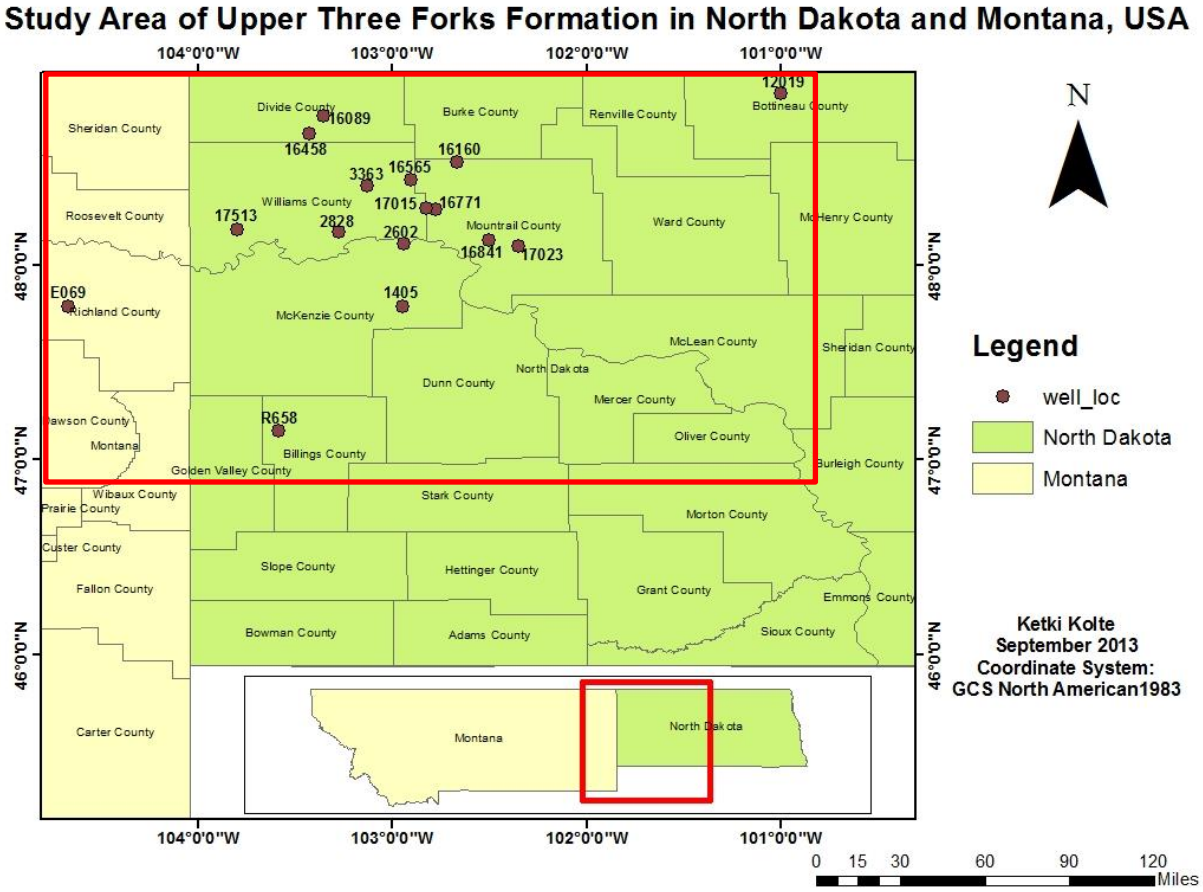

Figure 1: Well locations in the upper Three Forks Formation in western North Dakota and eastern Montana used in the study

CHAPTER 2: GEOLOGICAL SETTING

The Williston basin is located in western North Dakota, eastern Montana in the USA, and in southern Saskatchewan and Manitoba in Canada. It represents an intracratonic trough with a diameter of 560 km and an area of approximately 250,000 km^2 (Kent and Christopher, 1994). The sediment thickness in this basin is about 4900 m. Sedimentation in the Williston basin started during the Cambrian and has continued through the Quaternary period (Gerhard et al., 1990). The sediments mostly consist of limestones and dolomites along with some clastic sandstones, siltstones, mudstones and shales (Geologic Atlas, 1972). The highest rate of subsidence during the upper Devonian in the basin is represented by thick shallow-marine carbonates and evaporites along with minor amounts of silt and sand in varying proportions deposited in an extensive epeiric sea (LeFever, 2008). Globally, the paleo-climate of the Late Devonian is believed to be non-varyingly warm (Dickins, 1992). This warm climate is reflected by evaporites in the Three Forks Formation that occur as anhydrite nodules in red-colored siltstones and mudstones (Patterson and Kinsman, 1982; Berwick and Hendricks, 2011).

The Late Devonian Three Forks Formation (~385-360My) conformably lies above the Birdbear/Nisku Formation and below the lower Bakken shale member. The Pronghorn member, now considered a part of the Bakken Formation (LeFever et al., 2011) is locally present stratigraphically above the upper Three Forks Formation (Bentek Energy, 2012). The average thickness of the Three Forks Formation is about 150 ft (45 m) (Lexicon of Canadian Geologic Units, 2010). The Three Forks Formation thins in all directions away from the depocenter, which is located in Mountrail, Dunn and McKenzie counties of North Dakota (LeFever, 2008), and is characterized by an erosional unconformity at the top. In North Dakota, thinning of the formation

is observed prominently toward the basin margins in the east and towards the Cedar Creek anticline in the southwest (LeFever, 2008).

Sediments of the Three Forks Formation have traditionally been subdivided into six units (Christopher, 1961; Smith and Bustin, 2000), but Bottjer et al. (2011) and Egenhoff et al. (2011) differentiated three units within the Three Forks Formation based mostly on core work (for Bottjer et al., 2011, see Fig. 2). The lower unit consists of sandstones, siltstones, and mudstones with evaporites; the central portion of matrix-supported conglomerates with few centimeter-scale dolomite beds in-between (Egenhoff et al., 2010; L. Droege, 2014, personal communication); and the upper portion is characterized by bedded to massive dolomite containing varying amounts of greenish siliciclastic mudstones (Berwick and Hendricks, 2011; Bottjer et al., 2011). The succession is thought to be deposited in a sabkha-like (lower unit) to in part shallow subtidal environment (upper part; Berwick and Hendricks, 2011; L. Droege, 2014, personal communication) and reflects an overall deepening (Bottjer et al., 2011), although some models maintain that even the top portion was laid down in a sabkha-like setting without the influence of subtidal deposition (Berwick, 2008).

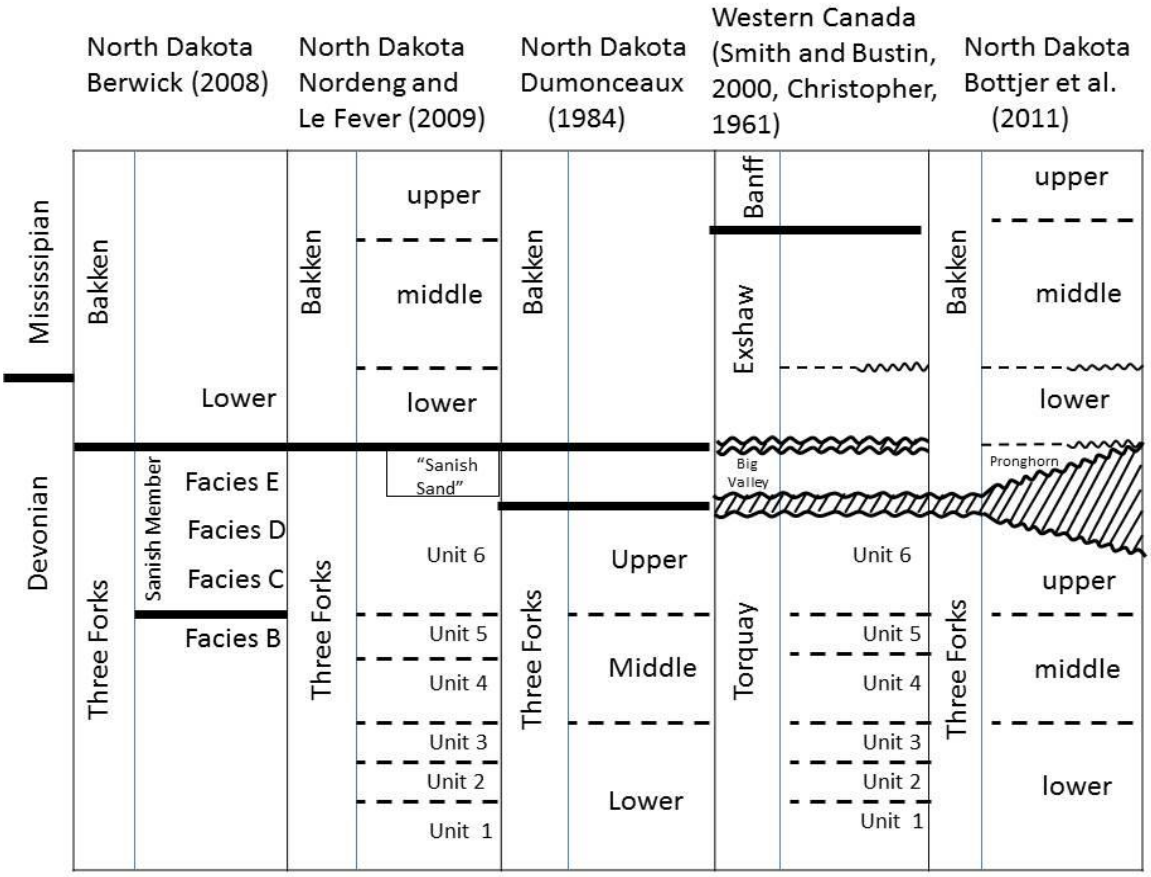

Figure 2: Nomenclature and correlation chart for the Three Forks and Bakken Formations, Williston Basin, North Dakota, Montana, and Canada (from Bottjer et al., 2011)

CHAPTER 3: METHODOLOGY

Forty-two samples for thin sections were collected from sixteen upper Three Forks Formation cores. Each core was sampled for the dolomitic portion, for it being the most targeted reservoir in the Upper Three Forks Formation (Nicolas, 2007). Fifteen of these cores are from the North Dakota portion of the basin while one core is from Montana. Two of these cores are stored at the Core Research Centre of the USGS in Denver, Colorado, and the remaining fourteen cores were documented at the North Dakota Geologic Survey's Laird Core and sample library in Grand Forks, North Dakota.

3.1 Core Logging:

Each core was logged in detail on a standard logging template. Observations were made and recorded from the original core prior to collecting the samples for thin sections. The measured sections includes entering the grain size of the respective lithology, detailed lithological description, facies identification, sedimentary structures, porosity estimations in percent, interpretation and grain size trends.

3.2 Estimation of Porosity:

An attempt has been made to estimate the pore volume contained in the rock by quantitative analysis and by describing the geometry and its likely formation (and relative timing) of these pores in detail.

3.3. Quantitative Mineralogical Analysis:

The microscope used for this study is a Leica optical research microscope that has a resolution in the range of millimeters to tens of micrometers and magnification ranging from 25X to 400X.

The method applied in this study to quantify mineral and cement abundance follows the classical approach of point counting. It places a theoretical grid of a minimum of 300 points over a representative part of the thin section and based on this determines the abundance of each mineral phase, cement or grain type in the selected thin section. The values of each phase, cement or grain, are given in percent after finishing the point counting process (Appendix I – Table 2).

Here, a slight modification of this approach was applied that takes into account the 3D-effect (Fig. 3) of mineral grains and cement phases leading to more precise values for each of the constituents. Porosity indicated by blue dye is subdivided into two different categories: (1) category one follows the classical approach and counts a spot as 100% porosity when the counting point lies over a spot with entirely blue dye; (2) however, if the point counting spot shows a blue color indicating porosity, but additionally the outline of a grain can still be recognized below, it is counted it as 50% porosity and 50% the mineralogy of the underlying grain or cement in order to account for both types of components. This modified approach results in significantly lower porosity values than the traditional method and will give a more accurate picture of the nature of primary and diagenetic phases in the Upper Three Forks Formation.

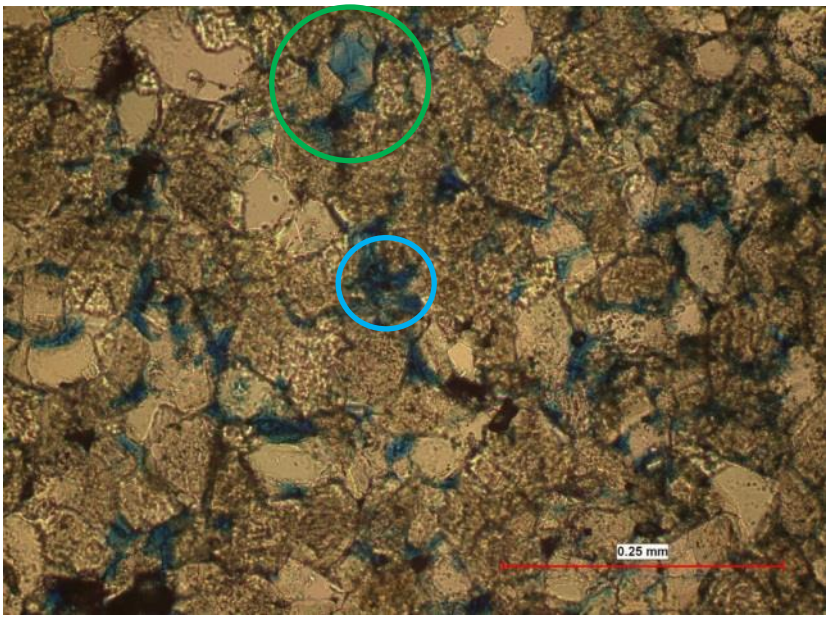

Figure 3: 3D-effect in grains and crystals [blue circle is representative of 100% porosity and green circle is representative of 50% porosity and 50% mineralogy]

3.4 Generation of Maps using GIS ArcMap:

Maps showing distribution of porosity and dolomite are created in ArcGIS using the Inverse Distance Weighting (IDW) tool. This method extrapolates values based on the spatial location of known points. The extrapolated values are assigned/calculated by the software based on arithmetic mean-average, wherein some data points contribute more than other data points to that average value (weighted average). Hence, certain points, especially if not surrounded by many other points have a stronger influence on the distribution of data on the maps than points that have close neighbors in their vicinity.

3.5 Scanning Electron Microprobe Analysis:

Eight thin sections of the upper Three Forks Formation were selected for Scanning Electron Microscope (SEM) studies at the USGS, Denver. The SEM process is a qualitative/semi quantitative analysis method to determine chemical composition. The SEM data is gathered from

the surface area at high resolution of a sample, and a 2D image is displayed on the connected monitors. Before analyzing the samples, they are coated with an approximately 15nm ultrathin carbon coating. Energy dispersive spectroscopy (EDS) is a method applied to recognize the elemental make-up of specific points of interest of a sample. In EDS, specific points of interest on the sample are "bombarded" with an electron beam inside a vacuum. An electron beam produces signals specific to the grains or minerals on which the beam is focused. These signals reflect the specimen's characteristics such as the chemical composition, surface texture, structure and arrangement of the components that constitute the sample (Goldstein, 2003).

3.6 Electron Microprobe Analysis:

One sample of the upper Three Forks Formation was selected for electron microprobe analysis. This analysis of a carbonate rock was obtained by using by JEOL 8900 using 10kv, 30nA beam electron microprobe at the USGS, Denver. The microprobe process is a quantitative analysis method, measuring the composition of a part of the sample. The beam of accelerated electrons generates X-rays with the aid of electromagnetic lenses. These X-rays enable determining the concentrations of specific elements in the sample, and display their abundance in the form of peaks. The peaks of a geochemical standard are matched with the peaks produced by the elements contained in the sample (Goldstein, 2003). For the upper Three Fork Formation sample investigated in this study, a standard was used containing the elements Ca (calcite), Mg (dolomite), Fe (hematite), Mn (rhodochrosite), S (barite), Si (quartz), Ba (barite) and Sr (celesite).

CHAPTER 4: RESULT – DESCRIPTIONS

The rocks of the upper Three Forks Formation consist of mostly dolomite crystals, here subdivided into dolomite I to VII phases representing successive stages of diagenetic alternations, along with anhydrite and pyrite crystals and detrital grains which are quartz, plagioclase, microcline, muscovite and clay.

4.1: Detrital Components

4.1.1. Quartz: Detrital quartz grains (Fig. 4A), both monocrystalline and polycrystalline (Fig. 4B) are found in all facies of the upper Three Forks Formation. These grains vary in size from 0.05 mm to 0.1mm (fine sand to coarse silt-size) in diameter. They are usually rounded to subrounded (Fig. 4.A), only a few being subangular to angular (Fig. 4C). In the upper Three Forks Formation, polycrystalline quartz is not as common as monocrystalline quartz grains. In some of the dolomitic beds, polycrystalline quartz is almost absent wheareas in places it can be up to 25% of the quartz. The total amount of detrital quartz in the upper Three Forks sediments varies between 0 and 53%. The monomict clast-supported conglomerate has generally slightly higher proportions (on average 24.61%) of detrital quartz compared to the intercalated massive to bedded dolomite (on average 23.54%).

4.1.2. Feldspar: Detrital feldspar, both plagioclase and microcline (Fig. 4D) is sparsely present in the upper Three Forks Formation. It makes up about 1 % of the total rock volume. Feldspars in the upper Three Forks Formation are normally rounded to subrounded (Fig. 4E). The average size of these detrital grains is 0.06mm (fine sand to coarse silt-size).

4.1.3. Clay: Clay constitutes of up to 30% of the rock volume. The clay content is usually lower in the monomict clast-supported conglomerate facies in comparison to that of intercalated

dolomites with mudstones. Clay occurs in two forms: as (1) Irregularly-shaped clay aggregates that are dark brown to black-colored, with in part non-distinct boundaries toward the dolomite crystals (Fig. 4F) and bright in the SEM (Fig. 4G); these aggregates range in size from 0.01 to 0.25 mm (fine sand size) that are either randomly oriented or dispersed along with the dolomite crystals; and as (2) clay clasts ranging in size from 0.25mm to 0.5mm (medium sand size), black in color that are rounded to subrounded in shape constituting solely or dominantly of clay (Fig. 4H).

4.1.4. Microdolomite Clasts: These are rounded to sub-rounded clasts dominantly made up of microdolomite crystals (0.02 to 0.05 mm – medium to coarse silt-size) along with clay aggregates (0.01 to 0.03mm – medium silt-size) (Fig. 4I). The size of these clasts can range from 0.25mm to 1.25mm (medium to very coarse sand size). The amount of these microdolomite clasts is highly variable but may constitute anywhere from 0 to 30% of the rock volume.

4.1.5. Muscovite: Muscovite is present in about one fifth of the thin sections. Muscovite grains vary from 0.025 to 0.05 mm in size (coarse silt-size). They often appear as small flakes or fibrous plates (Fig 4G). These flakes are arranged parallel to bedding and are usually present along bedding planes of deformed beds, though occasionally they may occur isolated and/or randomly oriented (Fig. 4J). Muscovite constitutes less than 3% of the rock volume.

4.1.6. Accessory Minerals / Heavy minerals: Subrounded to subangular colorless zircons and apatites (Fig. 4K) are sparsely present in the upper Three Forks thin sections. They constitute about 1 % or less of the rock volume.

4A

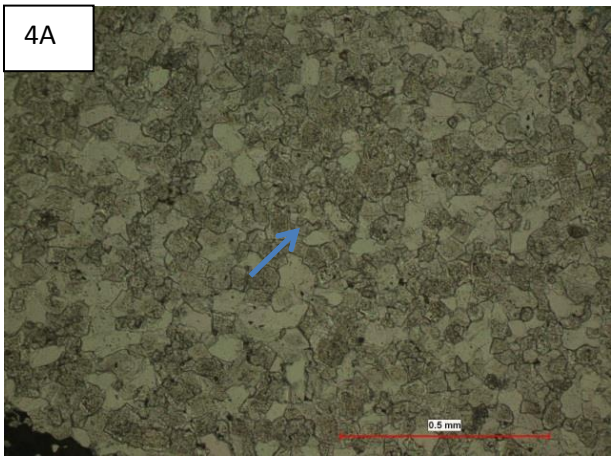

4B

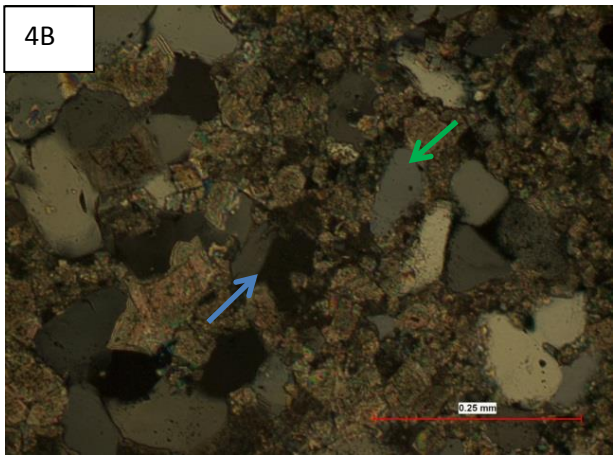

4C

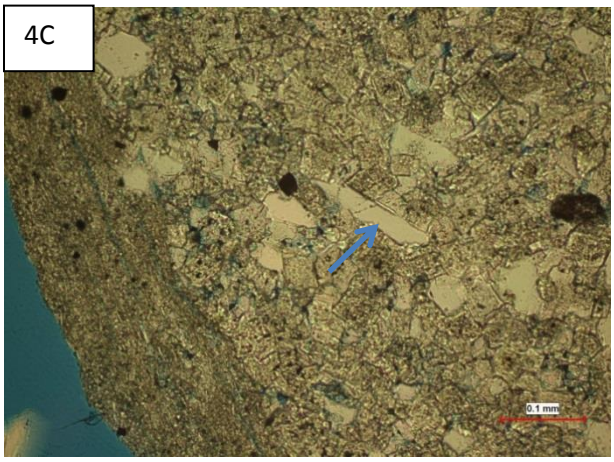

4D

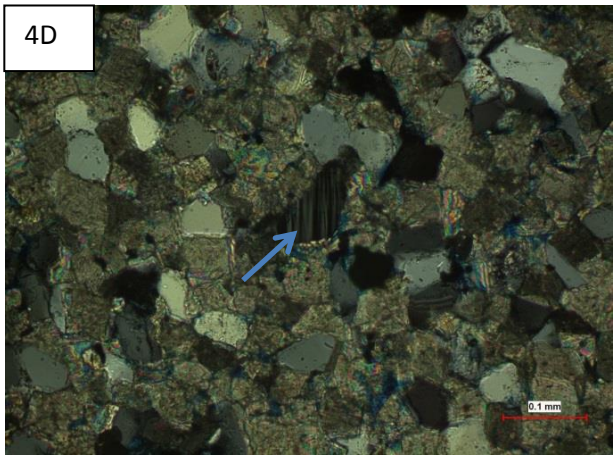

4E

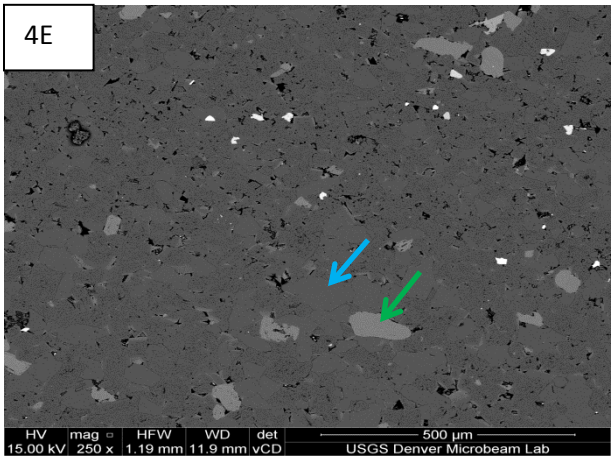

4F

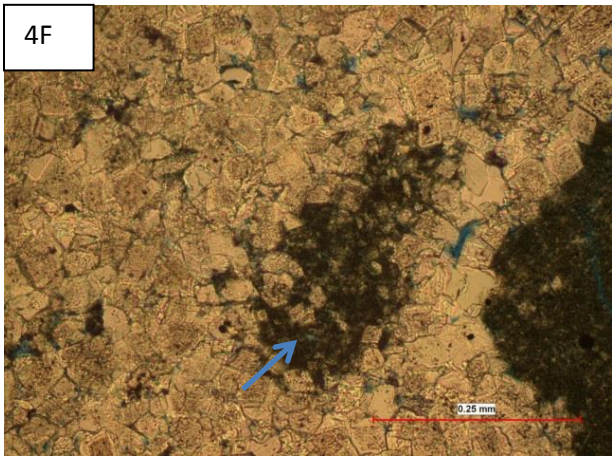

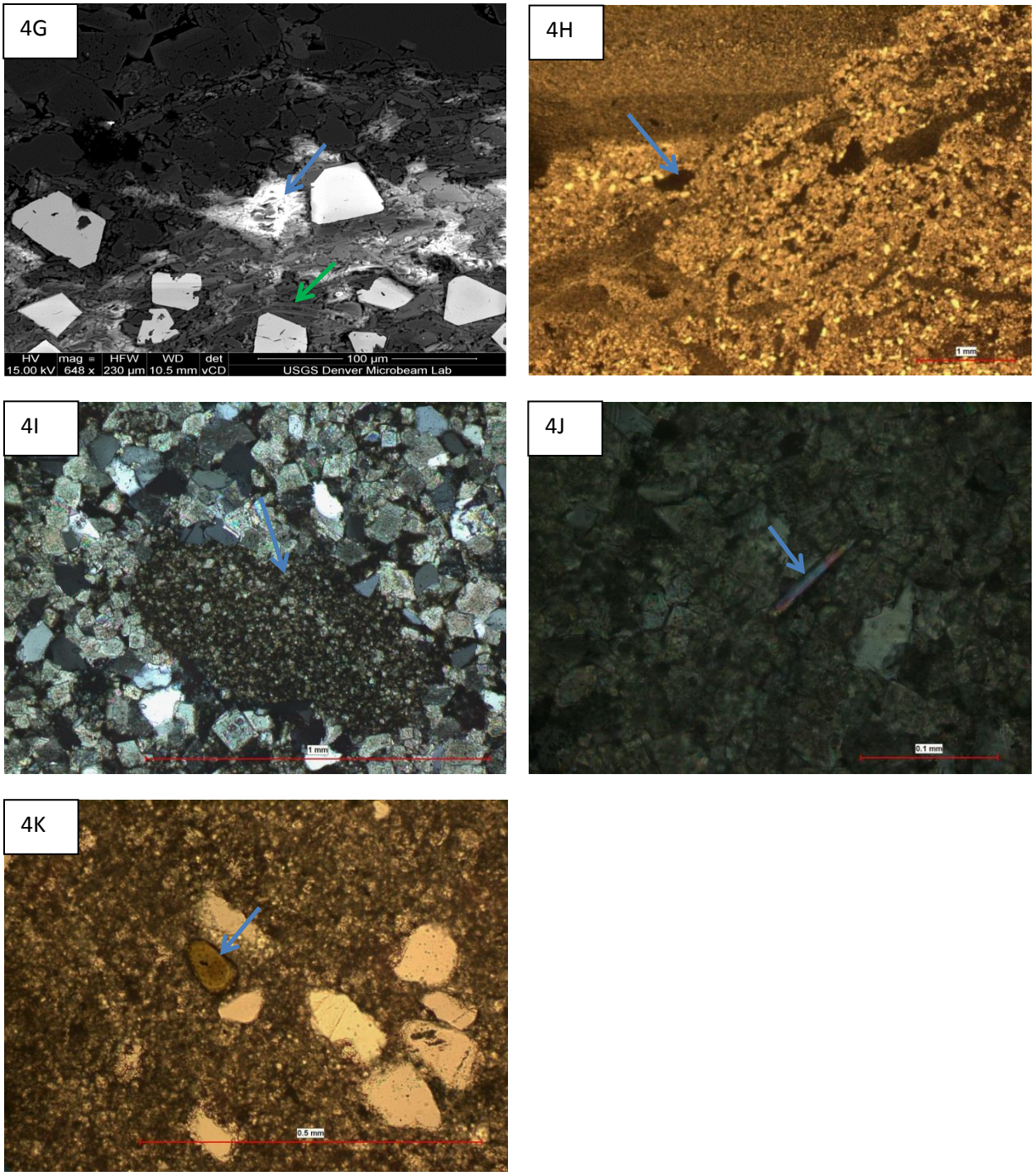

Figure 4: Detrital Photos from Thin Sections
4A Rounded to subrounded silt-size quartz grains surrounded by “dirty” inclusion-rich, very fine silt-size dolomite II rhombs (blue arrow); plane-polarized light. From core - Brigham O & G Olson 10-15-1H #17513 at 10696.3 ft (3260 m) depth.
4B Polycrystalline (blue arrow) and monocrystalline (green arrow) fine sand-size detrital quartz grains; cross-polarized light. From core - Hess Corporation EN-Rudland-156-94 3328 H-1 #16771 at 10436 ft (3180 m) depth.

4C Angular quartz grain (blue arrow) along with rounded to subrounded quartz grains; plane-polarized light. From core - Samson Resources Co Nordstog 14-23-161-98H #16089 at 8714 ft (2656 m) depth.
4D Very fine sand-size subrounded microcline feldspar grain (blue arrow); cross-polarized light. From core - Samson Resources Co Nordstog 14-23-161-98H #16089 at 8725.2 ft (2659 m) depth.
4E SEM Backscatter electron image showing prominent detrital quartz (blue arrow) and feldspar (green arrow) grains. From core - Whiting O&G Braaflat 11-11H # 17023 at 9991 ft (3045 m) depth.
4F Clay aggregate in silt-size dolomite (blue arrow); plane-polarized light. From core - Hess Corporation EN-Rudland-156-94 3328 H-1 #16771 at 10421.8 ft (3176 m) depth.
4G SEM image in which clay (blue arrow) appears bright in the form of tiny slightly elongate to irregularly shaped grains. Muscovite (green arrow) appears as long fibrous dark grains. Note the angular pyrite crystals. Headington Oil Co. From core - Nesson State 42X-36 #17015 at 10463.7 ft (3189 m) depth.
4H Clay clast in silt-size dolomite (blue arrow); plane-polarized light. From core - EOG Resources Bures 1-17H #12019 at 10611.7 ft (3234 m) depth.
4I Microdolomite clast along with clay aggregates present within it (blue arrow); plane-polarized light. From core - Gofor Oil Inc. Catherine E Peck 2 #1405 at 10822 ft (3298 m) depth.
4J Oriented muscovite grain at an angle to bedding (blue arrow); cross-polarized light. From core - Fidelity Exploration and Production Company Deadwood Canyon Ranch 43-28H #16841 at 10206 ft (3100 m) depth.
4K Heavy mineral (blue arrow), likely zircon; and surrounding silt-size grains consisting of mostly quartz; cross-polarized light. From core - Maxus Energy Short Fee 1-17H #R658 at 10489.1 ft (3197 m) depth.

4.2: Diagenetic Components

4.2.1. Dolomite:

4.2.1.1. Dolomite I: Dolomite I crystals are mostly euhedral, rhombic (Fig. 5A) or in places rounded to irregular (Fig. 5B). They occur as tiny cores 0.01 to 0.015 mm in size, generally with distinct and rarely with indistinct outlines. Dolomite I is dark, highly inclusion-rich and most of the times it is partly to entirely replaced by pyrite. In places, a dolomite I core may be partly dissolved (Fig. 5C) but can also partly maintain its rhombic shape.

4.2.1.2. Dolomite II: Dolomite II crystals are angular, rhombic (Fig. 5D) or irregularly shaped (Fig. 5E). They occur as large crystals 0.05- 0.06 mm in size, usually lacking well-defined edges but in places show the original rhombic crystal shape. Dolomite II is cloudy in appearance and

contains most likely abundant fluid and clay inclusions. This dolomite shows distinct outlines and is mostly anhedral though some dolomite II crystals are euhedral. Dolomite II also occurs as crystals of 0.01 to 0.02 mm (medium silt-size) in size in the form of minute crystal aggregates/clusters (Fig. 5F), often arranged within individual dolomitic laminae of approximately 0.025mm in thickness.

4.2.1.3. Dolomite III: Dolomite III consists of overgrowth and appears as relatively inclusion-poor to clean rims on dolomite II crystal rhombs (Fig. 5G, 5H and 5I). These rims are of uniform thickness but may vary in between the range of 0.007 to 0.03 mm in different crystals.

4.2.1.4. Dolomite IV: Dolomite IV consists of overgrowth on rims of dolomite III (Fig. 5J). Dolomite IV is an intermediate inclusion-rich phase though these rims may be equally inclusion-rich as dolomite II. The thickness of these rims ranges between 0.03 to 0.05mm. In some crystals where a dolomite IV rim is present as the last generation it sometimes shows an irregular outline.

4.2.1.5. Dolomite V: Dolomite V consists of clear inclusion-free rims that grow on dolomite IV and have thicknesses similar to dolomite III in the range of 0.007 to 0.03 mm (Fig. 5J). These rims are rare and if present are not very well-defined.

4.2.1.6. Dolomite VI: Dolomite VI occurs as an overgrowth on rims of dolomite V. This phase is also inclusion-rich like II and IV. The thickness of this rim ranges between 0.03 to 0.06 mm. In places, the boundaries of this phase may not be distinct (Fig. 5J).

4.2.1.7. Dolomite VII: These dolomite crystals occur as clear, angular rhombs devoid of inclusions. These rhombs have a size of 1mm or greater. They often occur as individual, perfectly euhedral crystals, only precipitating in vuggy pore spaces (Fig. 5K and 5L), but not as rims growing on other dolomite phases.

Electron microprobe analysis yielded Fe values in dolomites in the following ranges (i) 0.2 to 0.5 FeOWt% (Fig. 5M {points 1, 3 and 4} and Appendix I - Table 3) (ii) 0.9 to 1.3 FeOWt% (Fig. 5M {points 5 or 6} and Appendix I - Table 3) and (iii) 9.9 to 12.6 FeOWT% (Fig. 5M {points 7-13} and Appendix I - Table 3). These electron microprobe measurements indicate that the relatively inclusion-rich dolomites (dolomite II, IV and VI) have a low iron content, in the range of 0.2 to 0.5 FeOWt%; and the relatively inclusion-poor dolomite rims (dolomite III and V) have a higher iron content in the range of 0.9 to 1.3 FeOWt%; the clear dolomite VII has an iron content in the range of 9.9 to 12.6 FeOWt%.

4.2.2. Anhydrite: Anhydrite occurs as crystals of approximately 0.2mm – 0.5mm in length (Fig. 5N) and frequently forms blocky to lath-shaped crystals. The orientation of the lath-shaped crystals may sometimes be decussate (intersecting with each other) (Fig. 5O) with irregular margins. In places, several crystals of anhydrite can form one mass that may have inclusions of detrital quartz (Fig. 5P). Rarely, anhydrite may also exhibit preserved structures of dolomite (Fig. 5Q). Anhydrite varies in abundance between 0 to 9%.

4.2.3. Pyrite: Pyrite varies in abundance between 0 to 10%. It either occurs as cubes around 0.01mm in size (Fig. 5R) or may form irregular masses with a patchy appearance (Fig. 5S), in places aggregating into clumps of up to 1mm in diameter (Fig. 5T and 5U).

5A

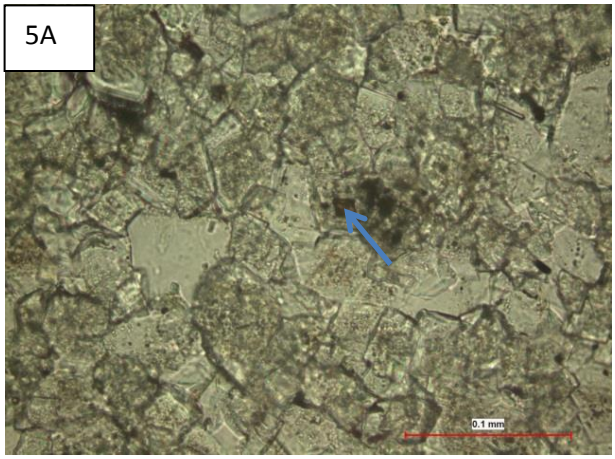

5B

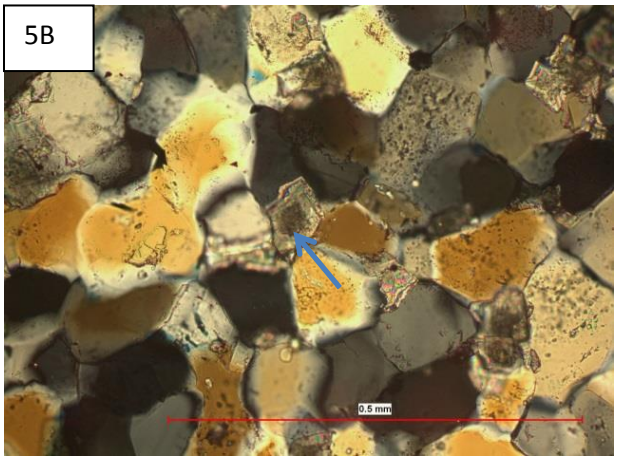

5C

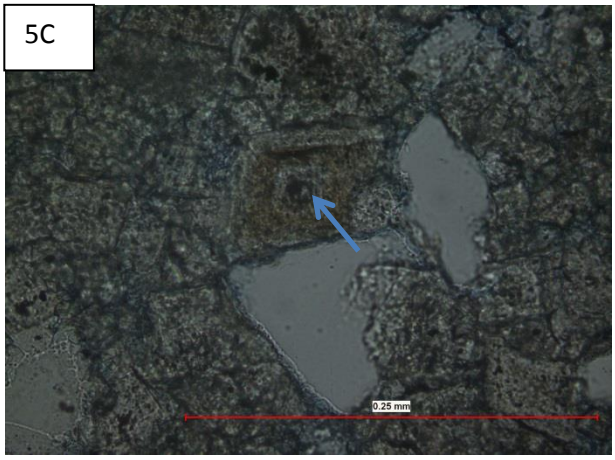

5D

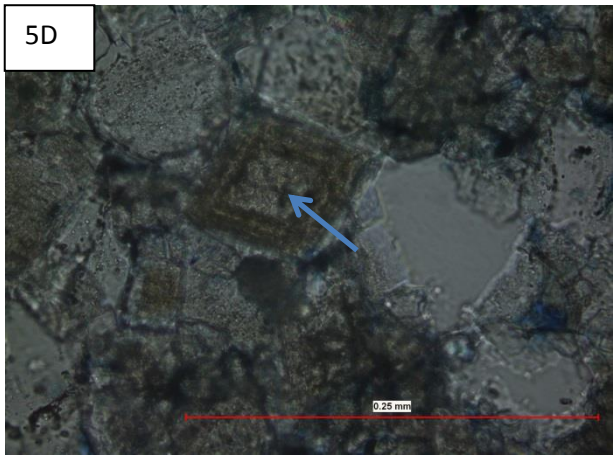

5E

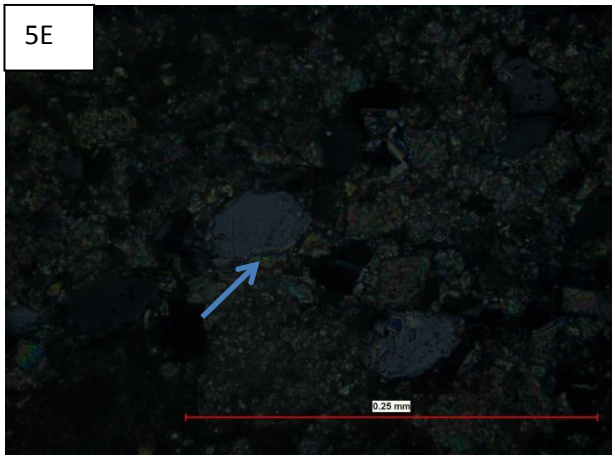

5F

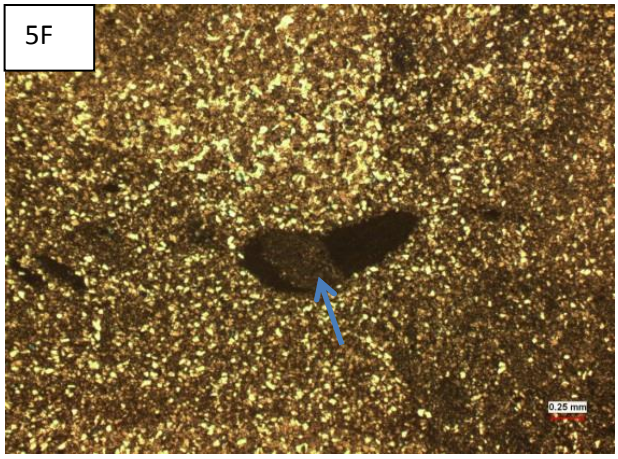

5G

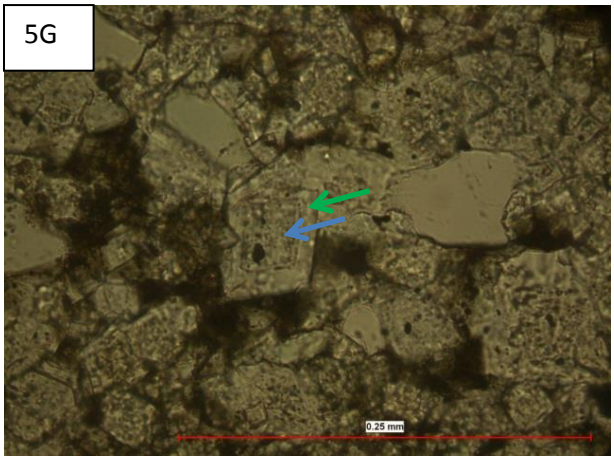

5H

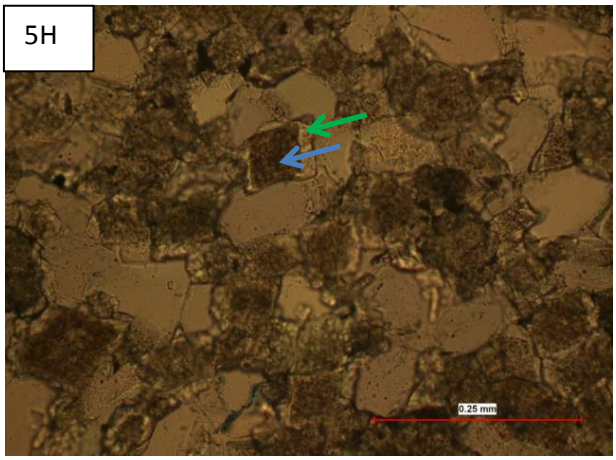

5I

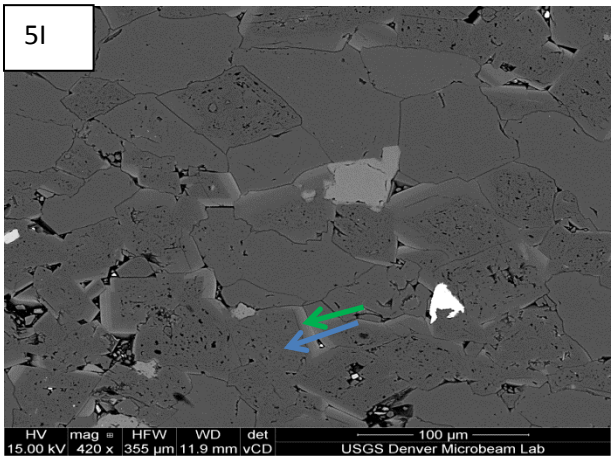

5J

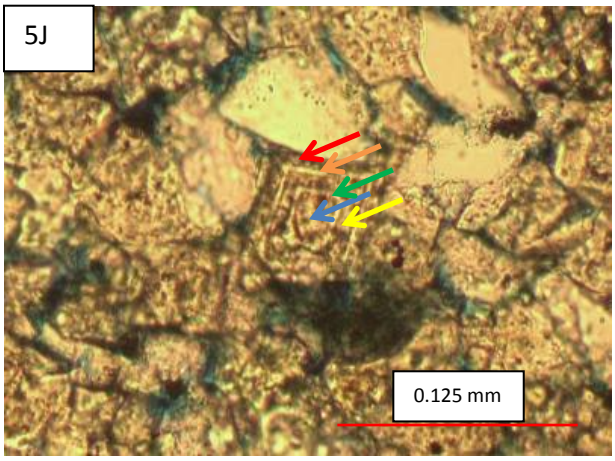

5K

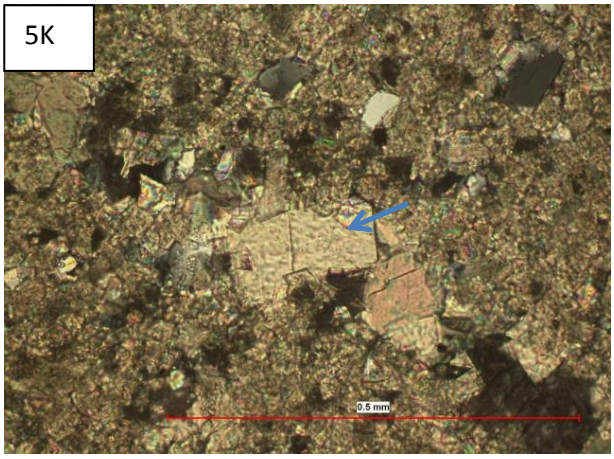

5L

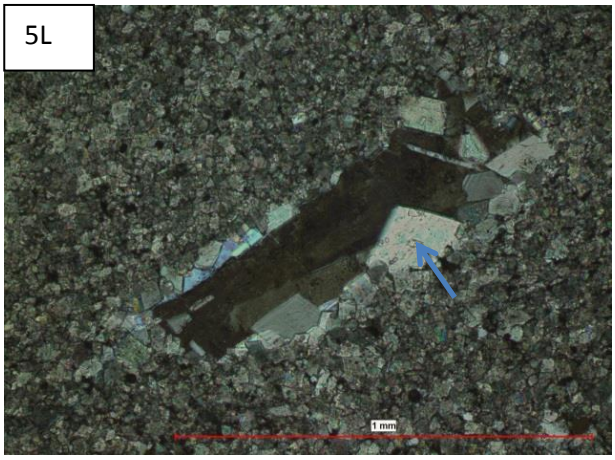

5M

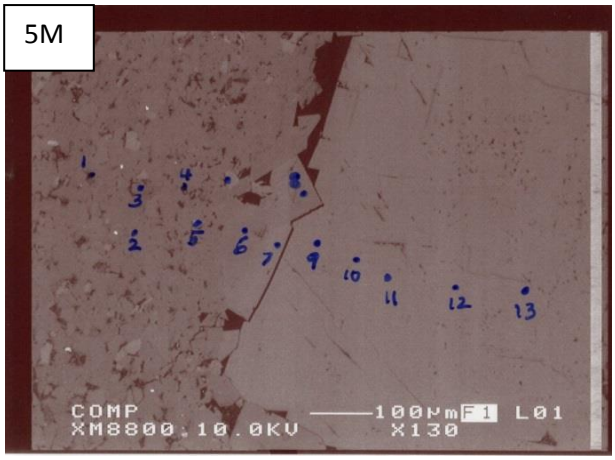

5N

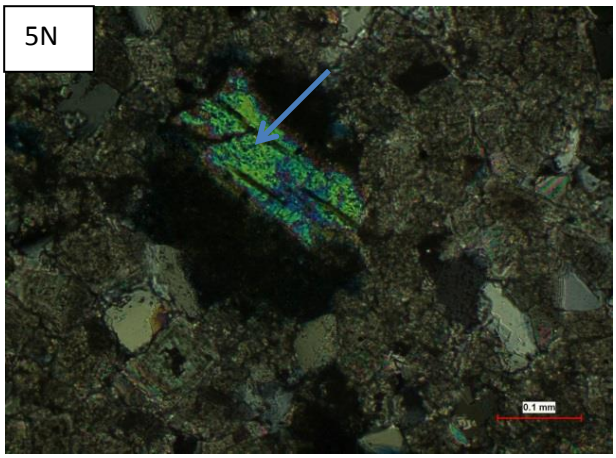

5O

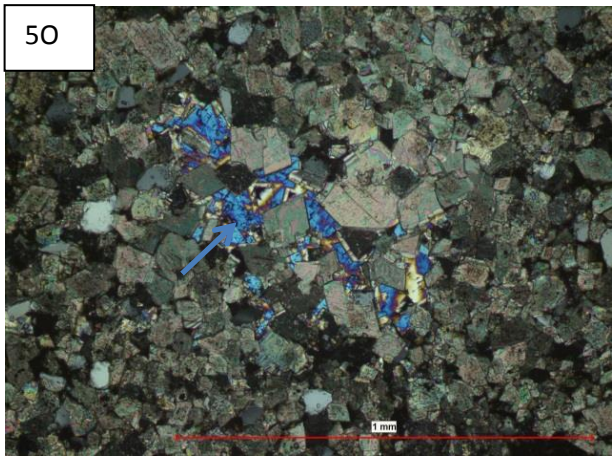

5P

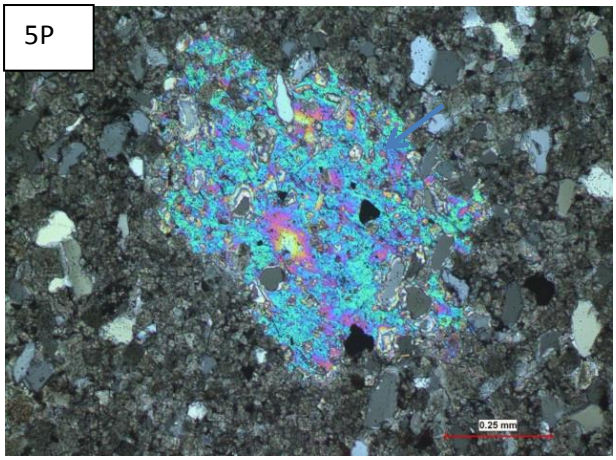

5Q

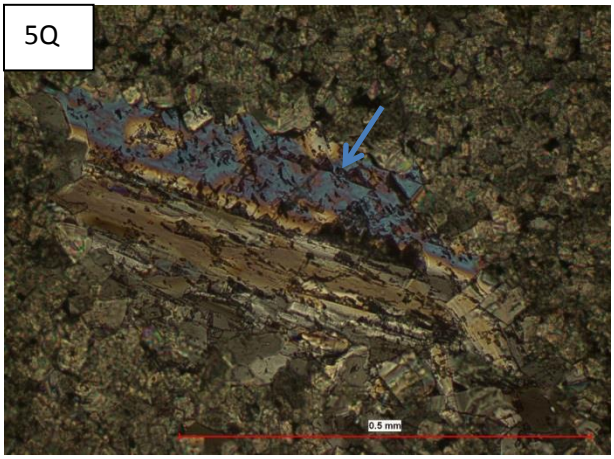

5R

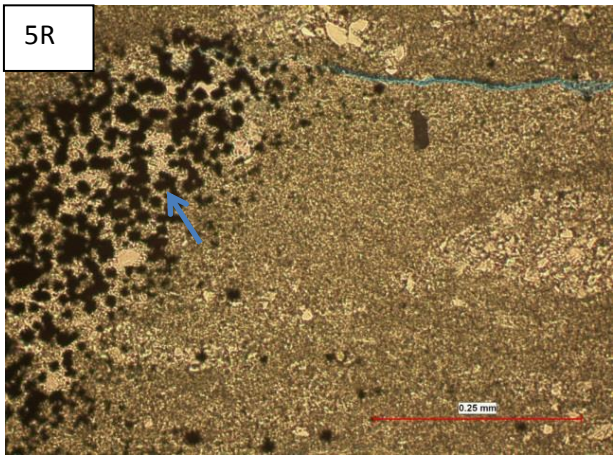

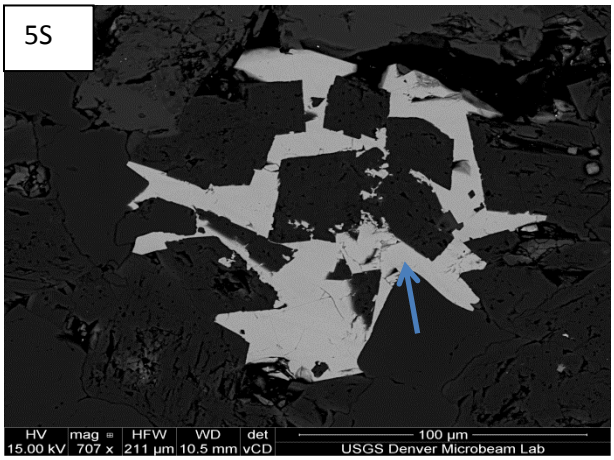

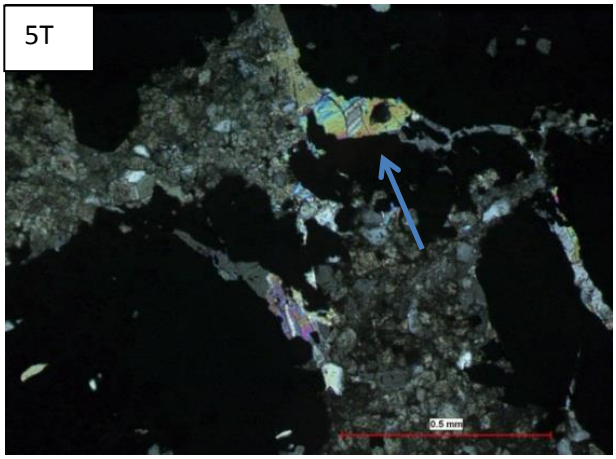

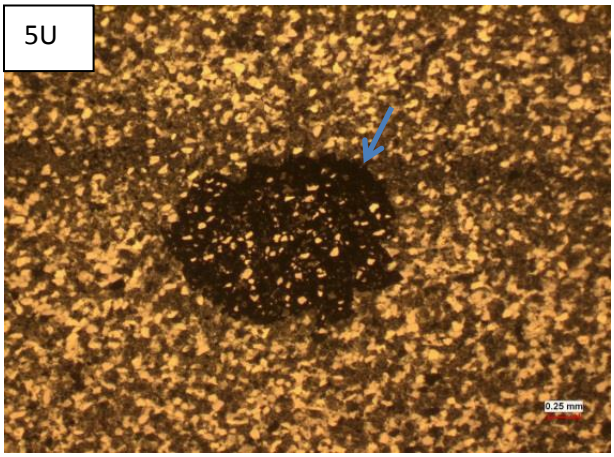

Figure 5: Diagenetic Photos from Thin Sections
5A Rhombic dolomite I core (blue arrow); plane-polarized light. From core - Fidelity Exploration and Production Company Deadwood Canyon #16841 at 10206 ft (3111 m) depth.
5B Subangular to subrounded dolomite I core in dolomite crystal (blue arrow); cross-polarized light. From core - Maxus Energy Short Fee 1-17H #R658 at 10489.1 ft (3197 m) depth.
5C Dolomite I core included and partly dissolved (blue arrow); plane-polarized light. From core - Samson Resources Co. Nordstog 14-23-161-98H #16089 at 8714 ft (2656 m) depth.
5D Type dolomite II rhombic crystal (blue arrow); plane-polarized light. From core - Hess Corporation EN-Rudland -156-94-3328 H-1 # 16771 at 10436 ft (3180 m) depth.
5E Subangular to irregular dolomite II replacing polycrystalline quartz (blue arrow); cross-polarized light. From core - Maxus Energy Short Fee 1-17H #R658 at 10489.1 ft (3197 m) depth.
5F Dolomite II crystals in mud clast (blue arrow); plane-polarized light. From core - Petro Hunt LLC Willard Johnson Trust 24B-2-1H #16458 at 9235.7 ft (2815 m) depth.
5G Dolomite III (green arrow) overgrowth on dolomite II (blue arrow); dolomite III retains the form of the previous generation dolomite on which it is seen to grow; plane-polarized light. From core - EOG Resources Bures 1-17H #12019 at 10611.7 ft (3234 m) depth.
5H Dolomite III (green arrow) overgrowth on dolomite II (blue arrow); inclusion-poor/clear versus inclusion-rich respectively; plane- polarized light. From core - Hess Corporation EN-Rudland-156-94 3328 H-1 #16771 at 10436b ft (3180 m) depth.

5I SEM image of dolomite rhombs exhibiting two zones. The outer zone (green arrow) appear brighter and clearer than inner zone (blue arrow). From core - Whiting O&G Braaflat 11-11H 17023 at 9991 ft (3045 m) depth.
5J Dolomite crystal showing 5 generations/phases of dolomite II to VI (II-blue arrow, III-green arrow, IV-yellow arrow, V-orange arrow, VI-red arrow); plane-polarized light. From core - Hess Corporation H. Bakken 12-07 16565 at 9743.6 ft (2969 m) depth.
5K Dolomite VII rhombs developing in open pores (blue arrow). Note that the late phase dolomite is clear, inclusion free, displays few cleavages, and have relatively larger crystal size than the previous dolomite generations, in cross-polarized light. From core - Cenergy Incorporated 1-4 Williams #E069 at 10073.2 ft (3070 m) depth.
5L Euhedral dolomite VII crystals growing in and filling up open pore space (blue arrow), in cross-polarized light. From core - EOG Resources Bures 1-17H #12019 at 10609.8 ft (3233 m) depth.
5M Electron microprobe SEM photo of different dolomite generations examined for iron content (Also see Appendix I – Table 3). From core - EOG Resources Bures 1-17H # 12019 at 10609.8 ft (3233 m) depth.
5N Subangular to irregularly shaped anhydrite replacing dolomite crystals (blue arrow); in cross-polarized light. From core - Cenergy Incorporated 1-4 Williams #E069 at 10077.2 ft (3071 m) depth.
5O Late stage decussate anhydrite crystals in secondary open pore spaces (blue arrow), in cross-polarized light. From core - EOG Resources Bures 1-17H #12019 at 10611.7 ft (3234 m) depth.
5P Anhydrite replacing most likely dolomite cements leaving the quartz and pyrite component unaltered (blue arrow), in cross-polarized light. From core - Headington Oil Co. Nesson State 42X-36 #17015 at 10463.7 ft (3189 m) depth.
5Q Anhydrite replacing dolomite VII crystals. This late stage anhydrite preserves the features of dolomite in it (blue arrow), in cross-polarized light. From core - EOG Resources Bures 1-17H #12019 at 10609.8 ft (3233 m) depth.
5R Mineralization of individual pyrite crystals in the dolomitic rock (blue arrow), plane-polarized light. From core - Petro Hunt LLC Deadwood Canyon Ranch 43-28H #16458 at 9219.4 ft (2810 m) depth.
5S SEM image of randomly oriented pyrite replacing dolomite rhombs (blue arrow). From core - Nesson State 42X-36 # 17015 at 10463.7 ft (3189 m) depth.
5T Patchy appearance of pyrite mineralization (blue arrow). Note pyritization engulfing and replacing the dolomite cements, partially the quartz and also anhydrite, in cross-polarized light. From core - Brigham O & G Olson 10-15-1H #17513 at 10696.3 ft (3260 m) depth.
5U Mineralization of pyrite, engulfing and replacing the dolomite cements, partially the quartz and also anhydrite, to form aggregates/clusters (blue arrow); plane-polarized light. From core - Hess Corporation EN Rudland 156-94 3328 H-1 #16771 at 10436b ft (3180 m) depth.

4.3: Porosity

The types of porosities described in the upper Three Forks Formation are based on the nomenclature and classification established by Choquette and Pray (1970). On average, the porosity in the upper Three Forks Formation is 5% but it varies from 0.33% to 13% (Appendix II

– Table 2). Open pore spaces in the upper Three Forks Formation can be up to 0.2 mm in diameter. The different types of porosities in the upper Three Forks are interparticle, intercrystalline, intracrystalline, moldic, fracture and vuggy porosity (Choquette and Pray, 1970) which are described below.

4.3.1. Interparticle porosity: This porosity type is present exclusively between detrital quartz grains (Fig. 6A). The size of these pores is on average approximately 0.02 to 0.03 mm. This porosity type is mostly present in the monomict clast-supported conglomerate facies, though it rarely also occurs in the other facies of the Upper Three Forks Formation. Interparticle porosity constitutes less than 2% of the rock volume.

4.3.2. Intercrystalline porosity: The size of these pores is generally about 0.03 to 0.06mm. Intercrystalline pores have irregularly variable shapes. They occur along the periphery of individual crystals (Fig. 6B). Intercrystalline porosity is the most frequently occurring type of porosity in all facies associations of the upper Three Forks Formation. This type of porosity is also observed between dolomite II crystals that are present in individual mud clasts (Fig. 6C). The amount of this porosity ranges between 0 to 10% in the upper Three Forks Formation.

4.3.3. Intracrystalline porosity: Intracrystalline porosity is abundant in upper Three Forks Formation thin sections. It occurs in all facies and facies associations, but more dominantly in the intercalated dolomites with clay-rich siliciclastic mudstone facies association. This type of porosity is frequently observed in the core portion of dolomite I crystals and also along their internal crystal boundaries in dolomite II (Fig. 6D). It also occurs in micrometer-size crystals that are present in microdolomite clasts (Fig. 6C). The intracrystalline pores are fairly common and are present randomly within the dolomitic crystals, rarely following the outline of the crystal.

These pores generally are of irregular shape and variable sizes. The pore size varies from 0.01 to 0.05 mm. On average, the pores are 0.2 mm in length and 0.1 mm in width, if elongate, and 0.02 mm in diameter, if rounded. This porosity ranges from 0 to 10% in the upper Three Forks Formation.

4.3.4. Moldic Porosity: In contrast to Choquette and Pray (1970) who defined "moldic porosity" exclusively as open pores within a rock resulting from the dissolution of coated or biogenic grains, here the term "moldic" is used to describe complete dissolution of all types of grains or crystals in the upper Three Forks Formation. This type of porosity forms dissolution pores between 0.08 and 0.1 mm in diameter which generally preserve the outer shape of the dissolved crystals (Fig. 6E). Moldic porosity is absent in some parts of the upper Three Forks Formation but can form up to 5% of the rock volume in places.

4.3.5. Fracture Porosity: Fractures developed in the upper Three Forks Formation are usually straight and range from 0.8 to 1.2 mm in length and 0.1 to 0.3 mm in width. These fractures are filled with anhydrite or late stage clear dolomite crystals (Fig. 6F). Fracture porosity is seen both perpendicular and parallel to bedding. This type of porosity is more common in the intercalated dolomites with clay-rich siliciclastic mudstone facies association, compared to that in the monomict clast-supported conglomerate. Fractures and fractures exhibiting porosity also occur confined to individual clay/mud clasts (Fig. 6G). The fractures within the mud clasts range from 1 to 1.25 mm in length and 0.03 to 0.04 mm in width, sometimes tapering towards the margin of the clay clast. Fracture porosity constitutes about 2-3% in the upper Three Forks Formation.

4.3.6. Vuggy Porosity: Vugs in the upper Three Forks Formation are of variable sizes ranging from 0.1 mm to 0.25 mm, and have rounded to irregular shapes (Fig. 6H). Vugs are common in

dolomites with clay-rich siliciclastic mudstone facies association of the upper Three Forks Formation and only occur rarely in other facies associations. These vuggy pores constitute between 1 to 2% of the rock volume. Vugs either occur as open pores or filled with clear dolomite and/or anhydrite crystals.

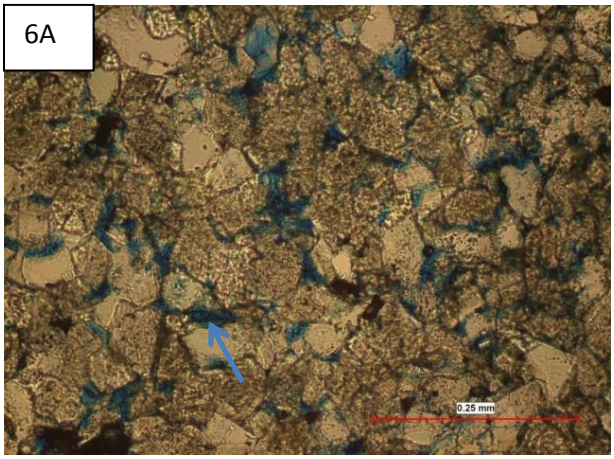

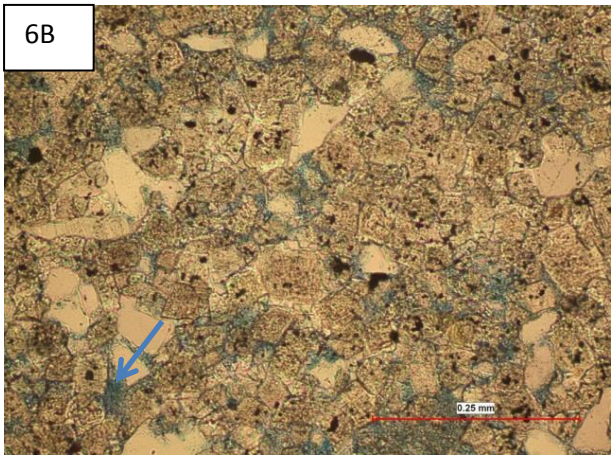

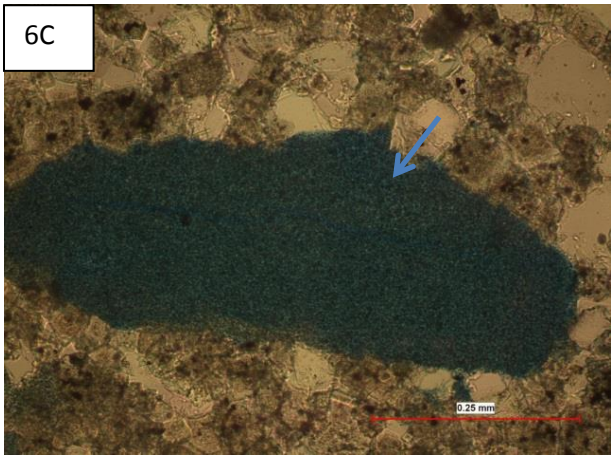

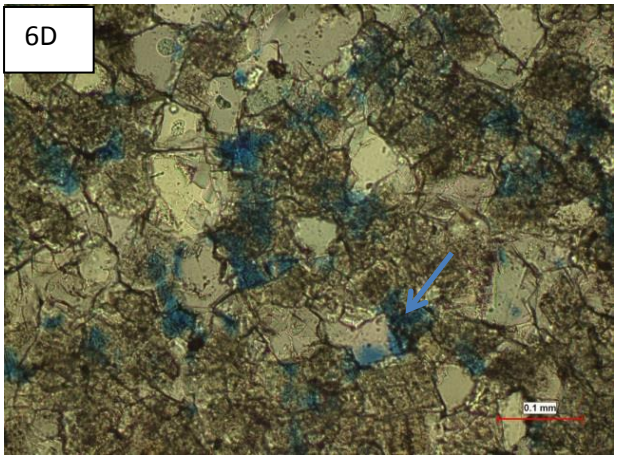

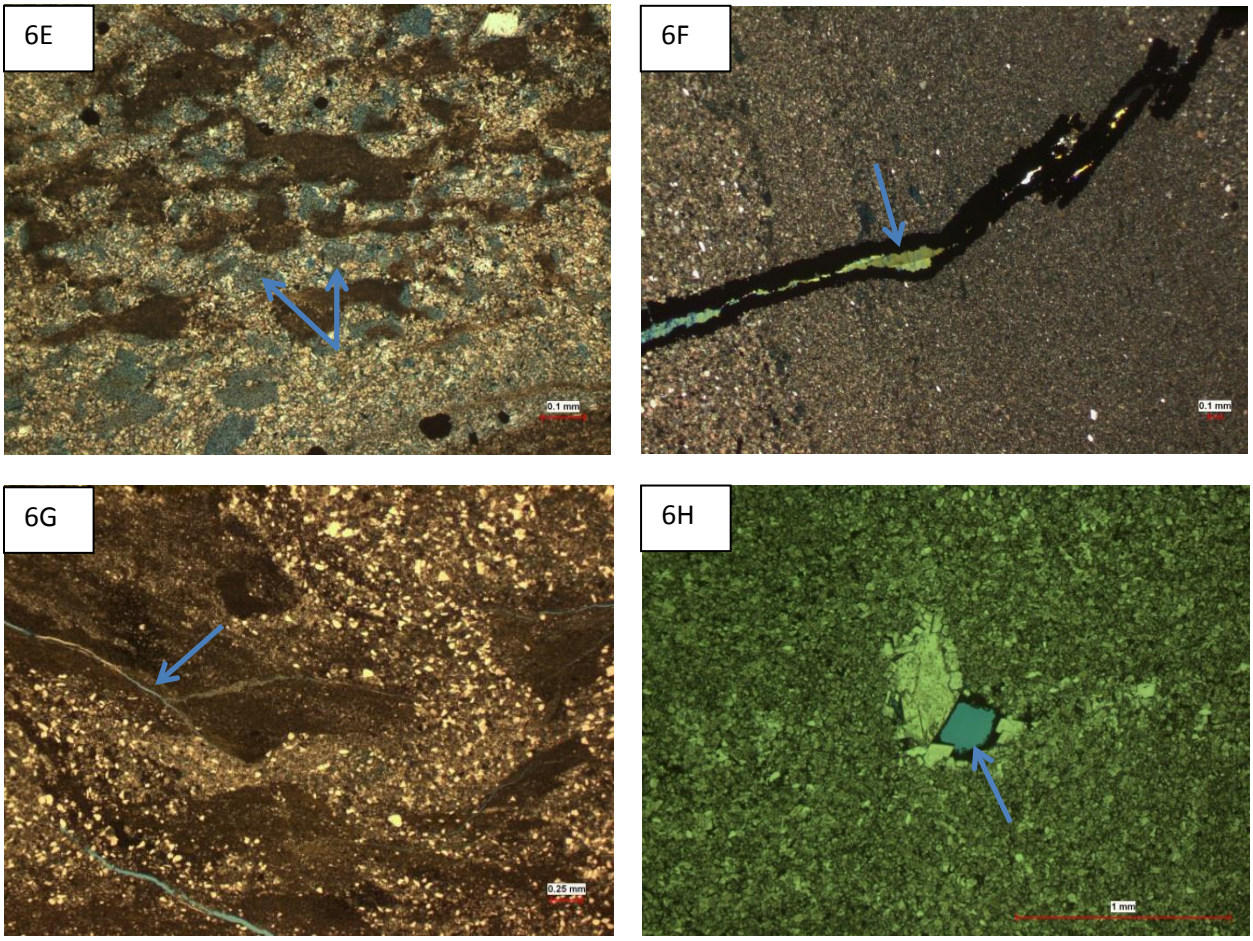

Figure 6: Porosity Photos from Thin Sections
6A Interparticle porosity between detrital quartz grains (blue arrow), plane-polarized light. From core - Petro Hunt LLC Willard Johnson Trust #16458 at 9235.7 ft (2815 m) depth.
6B Intercrystalline porosity between dolomite II crystals (blue arrow), plane-polarized light. From core - Petro Hunt LLC Willard Johnson Trust #16458 at 9219.4 ft (2810 m) depth.
6C Intercrystalline and intracrystalline porosity in mud clast (blue arrow), plane-polarized light. From core - Petro Hunt LLC Willard Johnson Trust #16458 at 9219.4 ft (2810 m) depth.
6D Intracrystalline porosity within porous dolomite cement crystals (blue arrow), plane-polarized light. From core - Cenergy Incorporated 1-4 Williams #E069 at 10077.2 ft (3071 m) depth.
6E Moldic porosity (blue arrows); note selective dissolution of dolomite crystals and detrital grains; plane-polarized light. From core - Samson Resources Nordstog 14-23-161-98H #16089 at 8714 ft (2656 m) depth.
6F Fracture porosity filled with late stage anhydrite cement (blue arrow), in cross-polarized light. From core - Samson Resources Nordstog 14-23-161-98H #16089 at 8417 ft (2656 m) depth.
6G Fracture porosity in mud clasts (blue arrow), plane-polarized light. From core - Petro Hunt LLC Willard Johnson Trust #16458 at 9219.4 ft (2810 m) depth.
6H Vuggy porosity (blue arrow), note the development of late stage dolomite cement in the open pore space, in plane-polarized light. From core - EOG Resources Bures 1-17H #12019 at 10609.8 ft (3234 m) depth.

4.4: Distribution and amount of dolomite in the upper Three Forks Formation

Figure 7 shows the distribution of dolomite in the study area based on point-counting of cores. It does not differentiate between the seven dolomite generations described in chapter 5.2.1 but lumps them all in to one group as it was impossible to separate them for point-counting purposes. In general, the amount of dolomite varies throughout the study areas and shows a patchy distribution with several highs and lows with values ranging from 35 to about 75%. Distinct strongly developed trends could not be detected. Nevertheless, the amount of dolomite shows three distinct highs located in the center of the study area on an E-W transect. Interestingly, the lowest values of dolomite concentration are also located in the central part of the study area aligned along a NNE-SSW-oriented zone. In general, both eastern and western portions of the study area show a very low data density and therefore those areas should be interpreted with caution. The center of the investigated area, however, reflects the variety in dolomite content over very short distances that can be present within the upper Three Forks Formation.

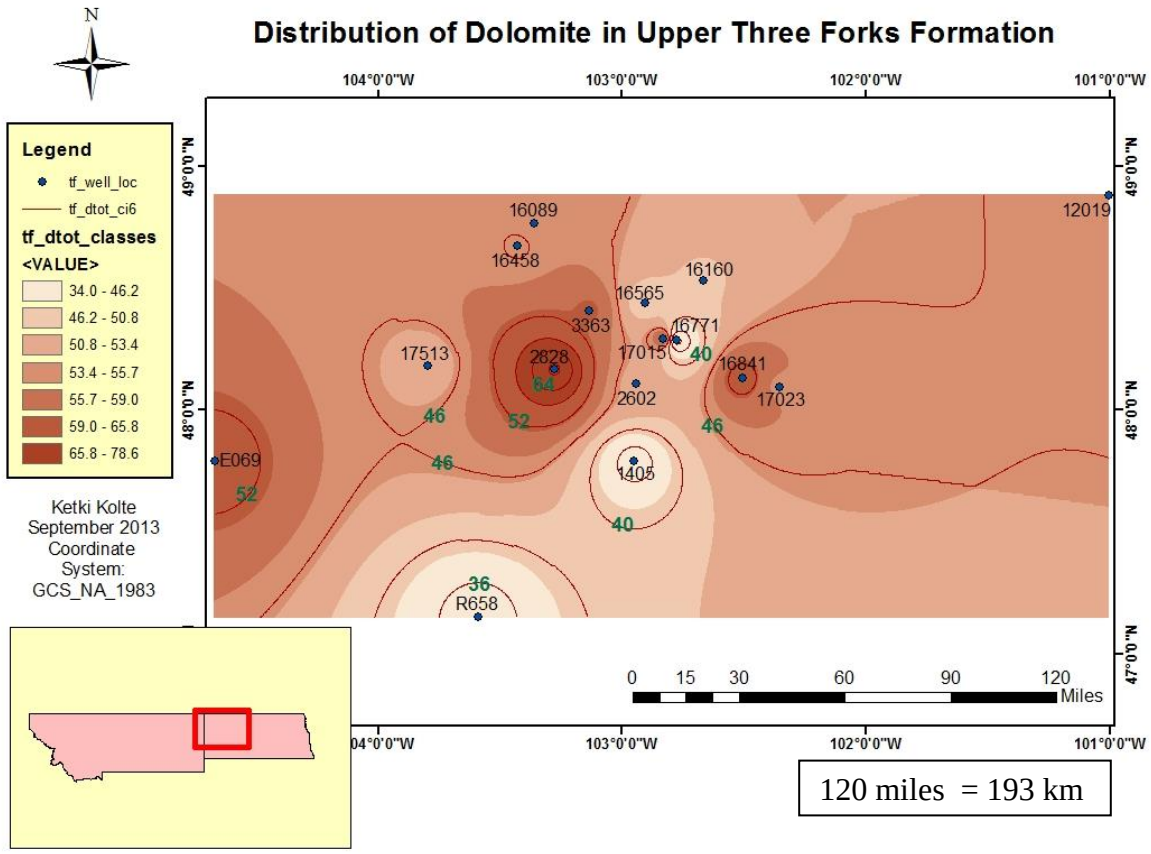

Figure 7: Map showing distribution of dolomite in the upper Three Forks Formation study area; contours represent percent dolomite (contour interval = 6); numbers posted at well locations are the Three Forks (tf) well ID names.

4.5: Distribution of porosity in the upper Three Forks Formation

As the dolomite, porosity is also unequally distributed throughout the upper Three Forks Formation in the study area varying between 2 and about 10% (Fig. 8). However, even though the data density is equally concentrated on the central parts of the study area largely leaving the west and east untouched, a clear trend with an increase of porosity from the E to the W is evident. Maximum values of 6 to about 12% however are found in wells between about 103°W and 104°W (Fig. 8) and not in the wells located furthest to the west. These values are arranged along an overall N-S-trending area that may have a slight inclination towards NNE-SSW.

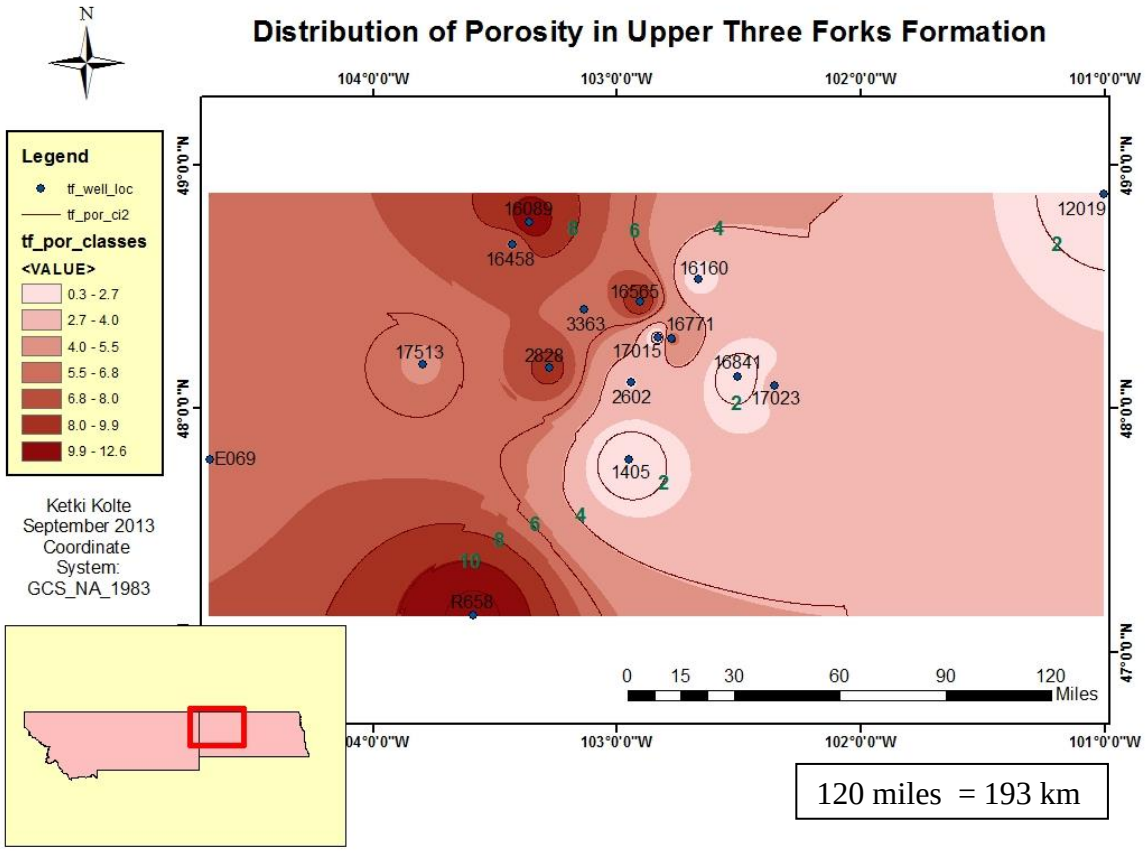

Figure 8: Map showing distribution of porosity in the upper Three Forks Formation study area; contours represent present porosity (contour interval = 2); numbers posted at well locations are the Three Forks (tf) well ID names.

CHAPTER 5: INTERPRETATIONS

The entire upper Three Forks Formation consists mostly of dolomite, and all dolomite from this unit, regardless which one of the seven generations it belongs to, is interpreted in this study as "secondary" or post-depositional. Also the different types of porosity in this unit formed after deposition and are therefore considered "secondary" except interparticle porosity (Fig. 9).

Based on its position generally in the center of several of the dolomite crystals in the upper Three Forks Formation, the Fe-rich dolomite or dolomite I is interpreted here to be the oldest of all of the dolomite cements, even though an absolute age cannot be assigned to this phase. It clearly predates dolomite II that always encases dolomite I crystals. The several micrometer-scale, also generally inclusion-rich dolomites that makes up the bulk of the rock in the upper Three Forks Formation are here interpreted to represent the same dolomite II as the larger crystals because of its similar habit, and because dolomite II, where it forms part of a crystal showing several generations of overgrowth, generally represents the thickest rim, indicating that this dolomitization event most likely affected larger parts if not most of the rocks in the upper Three Forks Formation. The generations of dolomite that form overgrowth rims on top of dolomite II are considered to represent cements that precipitated after most of the rock was transformed into dolomite II and post-dates dolomitization of the bulk of the upper Three Forks Formation. Dolomite generations III to VII form therefore, consecutive and subsequent growth stages onto selected dolomite II crystals. The fact that these five "late" stages of dolomite cements are overall rare in the succession combined with the generally low porosity values indicates that very little space remained in the rock in order to form overgrowth rims in many places leading to a very isolated presence of dolomite other than dolomite generation II.

The succession of alternating clear and inclusion-rich dolomites in dolomite generations II to VI reflects the changing chemistry of fluids passing through the upper Three Forks Formation during its diagenetic history. It also shows that none of these two dolomite types seems to be characteristic for a specific stage during diagenesis. In contrast, both chemical environments seem to constantly alternate during the upper Three Forks Formation's post-depositional history. However, the ion beam data shows that despite their outer appearance, the dolomite cements get more Fe-rich through time.

Relative cement successions show that most likely two different types of anhydrite occur in the upper Three Forks Formation: a crystalline anhydrite that exclusively replaces dolomite I and II, in places also incorporating detrital quartz grains as 'relict' structures, and a crystalline lath-shaped anhydrite that may replace all the dolomite generations. The late anhydrite, as it replaces even dolomite VII, must have been precipitated after deposition of all the dolomite phases and therefore reflects the last precipitation event during the diagenesis of the upper Three Forks Formation (Fig. 9). As both anhydrite types are generally rare throughout this unit it seems that anhydrite played a role only locally, most likely related to pathways that penetrated most of this unit and would allow anhydrite-rich fluids from the lower Three Forks Formation to pass upwards into the upper Three Forks Formation. It is therefore speculated here that the presence of anhydrite in upper Three Forks Formation thin sections likely indicates the vicinity to a fracture or fault that cuts several tens of meters down into the sulphate-rich base of the same unit. These fractures/fault were most likely not active during sedimentation but during later stages of burial.

Pyrite formation in the upper Three Forks Formation seems to have occurred in one to three phases that may be placed in a relative time order (Fig. 9). Dolomite II crystals that are replaced

by pyrite show a pyritization event that succeeds dolomite II formation; however, it is unclear whether this pyrite precipitation event is equivalent to later pyrite formation where this iron sulphite replaces dolomite VII and/or anhydrite (Fig. 5T).

Porosity formation in the upper Three Forks Formation is limited to several tens of a micron-size pores that occur exclusively in or associated with dolomite cements, and ranges between 0 and 12 % throughout the analyzed thin sections. Intercrystalline porosity occupies the place between individual dolomite crystals, generally dolomite II. Its formation is therefore most likely linked to the relatively early event forming dolomite II as dolomite formation from calcite generally produces up to 13% of porosity (Weyl, 1960). The intracrystalline porosity in dolomite generations II, IV and VI, in contrast, must have formed during dolomite precipitation as this porosity type is even preserved in crystals where the porosity-bearing dolomite phases are entirely covered by later non-porosity-containing dolomite generations. This dolomite type may be associated with fluids containing either anhydrite or organic matter that gets included into the dolomite crystals and leads to the subsequent formation of micron-scale pores (Jacka, 1984). While this porosity type is fairly abundant in the upper Three Forks Formation individual pores are not connected and therefore this porosity type will only to a very small degree influence the amount of hydrocarbons produced from this unit.

Interparticle porosity, rare throughout the succession, is the only primary porosity type present in the upper Three Forks Formation. It is only preserved in portions of the succession that contains enough primary quartz grains, and in places where a later dolomite cementation did not influence original pore space in-between depositional grains. Vugs present only locally in the upper Three Forks Formation originated prior to the formation of dolomite VII as this dolomite generation partly fills some of these dissolution pores. Moldic porosity, here used in a sense representing

dissolution of entire to nearly complete dolomite crystals, is difficult to put into a valid relative time frame as it may have occurred at any time during the diagenesis of the upper Three Forks Formation (Fig. 9).

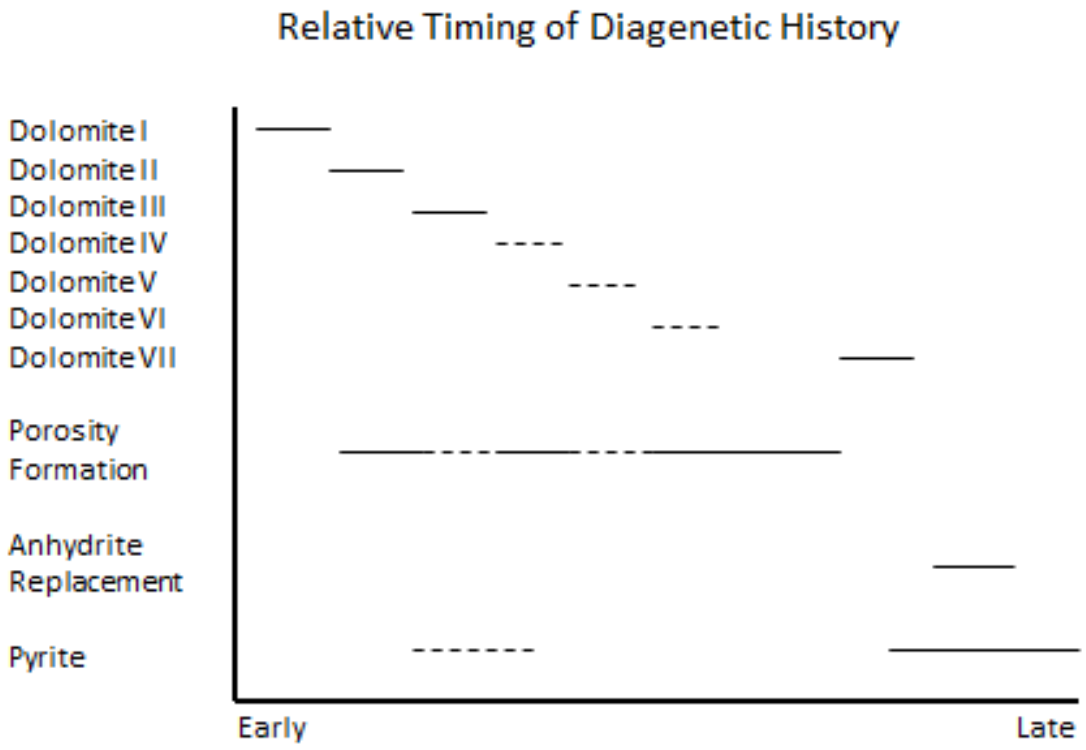

Figure 9: Relative Timing of Diagenetic Phases in the Diagenetic History of the Upper Three Forks Formation

CHAPTER 6: DISCUSSION

6.1: Inclusion-rich dolomites / Dolomite II, IV and VI:

In this study, it is assumed that most of the rock forming dolomite of the upper Three Forks Formation is represented by inclusion-rich dolomite II which often occurs in the form of rhombohedral crystals and subsequently by the later developing dolomite phases growing in the form of rims over it. However, its exclusive appearance as crystals supporting the assumption that most of the inclusion-rich dolomite in the upper Three Forks Formation is indeed dolomite II while at least parts of the inclusion-rich dolomites occurring as rock-forming could also in principle represent dolomite IV or VI. It is difficult to make a clear argument for or against this assumption. Nevertheless, it would be most likely that the initial formation of dolomite II affected most of the rock and not just the few crystals where this type of dolomite is unequivocally identified. The rhombohedral crystals also never have inclusion-poor centers but in places show a dolomite I iron-rich interior which may be taken as an argument that these are rather dolomite II than dolomite IV or VI crystals. Based on these two observations it seems more likely that dolomite II forms the bulk of the upper Three Forks Formation, and that dolomite IV and VI occur only as additional phases in very small amounts.

6.2: Real versus preparation-induced porosity:

In this study, it was assumed that the dye blue resin found in thin section represented original porosity present in the rock in the subsurface, and that the variation of this porosity in representative thin sections would reflect porosity changes in the upper Three Forks Formation through the basin. However, recent studies in the stratigraphically adjacent middle Bakken member (Egenhoff et al., 2013) suggest that at least a portion of the porosity described as present

in the rock is most likely preparation-induced and therefore not a characteristic of the original rock texture. This is corroborated by the fact that (1) many suspect pores still show the outlines of either the detrital grains or, in rare cases, the crystals that have been pulled out during the preparation process, or (2) the three porosity types that make up the bulk of open space in the upper Three Forks Formation are directly linked to dolomite or the space between dolomite crystals, yet there is no obvious relationship between the distribution pattern of dolomite and porosity. It is therefore most likely that the porosity distribution maps presented in the present study show values that are much higher than the real amounts of porosity present in the Three Forks Formation, and that the amount of detrital grains plugged from these rocks during preparation likely skewed the distribution patterns to a point where any relationship between the two parameters is not easily detected in this dataset any more. Nevertheless, assuming that the upper Three Forks Formation contains higher amounts of offshore facies in the centre of the basin and likely more shoreface and foreshore facies towards marginal area, the amounts of detrital grains should overall decrease towards the basin center and therewith towards the west within the study area. It is therefore probable that the general increase in porosity towards the west is to a degree real and not entirely artificially produced only by preparation of the thin sections.

6.3: Porosity distribution and its relation to dolomite:

The porosity distribution in the upper Three Forks Formation varies geographically across the Williston basin with the north-south-oriented maximum of up to 12.6% around 103.5° to 104°W. This is unexpected as most of the porosity observed was located in dolomite crystals or is associated with dolomite, yet there seems to be no inverse relationship between these two parameters as would be expected.

It is therefore most likely that the relationship between porosity and dolomite is not simple and most likely a combination of several factors, not simply a function of dissolution of the dolomite phase. This is also reflected in the different types of porosity present in the upper Three Forks Formation: intercrystalline porosity is thought of as resulting from replacement of an original calcite phase by dolomite (e.g. Choquette and Pray, 1970), and intracrystalline porosity seems to be directly related to the formation of certain dolomites themselves, not to a dissolution event. Vugs represent the only porosity type that is entirely formed from dolomite dissolution, yet it is relatively uncommon, and therefore most likely has a minor impact on the overall distribution pattern.

Also fractures, whether tectonically or load-induced added to the porosity distribution patterns shown in Figure 8. Even though these features do not account for much porosity, they represent a porosity type independent of dolomite dissolution, and considering the very low amounts of porosity in these rocks and in some of the thin sections may have considerably contributed to the overall amount of pores in these rocks (cf. Dow, 1974; Wilson et al., 1990; Purser et al., 1994).

CHAPTER 7: CONCLUSIONS

1. The upper Three Forks Formation shows seven recognizable dolomite diagenetic phases (Dolomite I to Dolomite VII) along with anhydrite and pyrite phases in the diagenetic succession. The upper Three Forks Formation rocks consist of dolomite II as the primary rock-forming mineral. Rare occurrence of dolomite III to VII is visible throughout the succession. Anhydrite is the last stage in diagenesis of the upper Three Forks as it replaces the late dolomite VII phase.
2. Several types of porosities also form part of the upper Three Forks diagenesis, of which intercrystalline, intracrystalline and moldic porosity types are the most common, while the interparticle, vuggy and fracture porosity types are relatively rare.
3. The porosity of the upper Three Forks Formation is nearly entirely secondarily developed except for the interparticle porosity. The intercrystalline porosity is a result of replacement diagenesis, intracrystalline porosity is developed along with the formation of dolomite cement phases, vuggy porosity and moldic porosity is created as a consequence of dissolution of dolomite crystals and fracture porosity reflects brittle rock behavior caused during burial.
4. Quantitative analysis of thin sections estimates 5 percent as the average porosity in the upper Three Forks Formation. Thus, the upper Three Forks Formation is by and large a tight reservoir, though at some places the porosity may be as high as 12 to 13 percent or as flat as 0 percent. Though the porosity distribution is uneven throughout, the overall trend shows that the porosity increases from east to west in the study area (Fig. 8).
5. Quantitative data reveals that the pore volume percentage is generally higher (2% to 11.66%) in the basal section of the upper Three Forks Formation compared to the overlying intercalated laminated dolomite beds (0.33% to 10.33%).

6. Geospatial maps generated from ArcMap may not be an ideal representation of the distribution of cements and porosity as it does not take into account the locally influencing geological factors subject to the study area and/or the sparse data density. Hence, the generated maps should only be used as a guideline to a generic understanding of the distribution trends (Appendix I-Table 2).

BIBLIOGRAPHY

Beitsch, R., 2010, Three Forks formation to yield lots of oil in North Dakota, Bismarck Tribune, April, http://bismarcktribune.com/news/state-and-regional/three-forks-formation-to-yield-lots-of-oil-in-north/article_368dcb38-53ef-11df-a6c8-001cc4c03286.html (accessed March 31, 2013).

Bentek Energy, 2012, The Williston Basin: Greasing the Gears for Growth in North Dakota, North Dakota Pipeline Authority, July, http://ndpipelines.files.wordpress.com/2012/07/bentek-nat-gas-study-july-25-2012.pdf (accessed May 29 2013).

Berwick, B.R., 2008, Depositional environment, mineralogy, and sequence stratigraphy of the Late Devonian Sanish Member (Upper Three Forks), Williston Basin, North Dakota, Master's Thesis, Colorado School of Mines, Golden, Colorado, 262 p.

Berwick, B., and Hendricks, M.L., 2011, Depositional Lithofacies of the Upper Devonian Three Forks Formation and the Grassy Butte Member of the Lower Bakken Shale in the Williston Basin, Bakken Guidebook, Chapter 7. The Bakken-Three Forks Petroleum System in the Williston Basin, John W. Robinson, Julie A. LeFever, Stephanie B. Gaswirth, eds. Denver, Colo.: Rocky Mountain Association of Geologists, p. 159-172.

Bottjer, R.J., Grau, A., Sterling, R., and Dea, P., 2011, Stratigraphic Relationships and Reservoir Quality at the Three Forks-Bakken Unconformity, Williston Basin, North Dakota, Bakken Guidebook, Chapter 8. The Bakken-Three Forks Petroleum System in the Williston Basin, John W. Robinson, Julie A. LeFever, Stephanie B. Gaswirth, eds. Denver, Colo.: Rocky Mountain Association of Geologists, p. 173-228.

Choquette, P.W., and Pray, L.C., 1970, Geologic Nomenclature and Classification of Porosity in Sedimentary Carbonates, American Association of Petroleum Geologists Bulletin, v. 54, p. 207-250.

Christopher, J.E., 1961, Transitional Devonian-Mississippian formations of southern Saskatchewan, Saskatchewan Department of Mineral Resources, Report 66, 103 p.

Dickins, J.M., 1993, Climate of Late Devonian to Triassic, Palaeogeography, Palaeoclimatology, Paleoecology, v. 100, p. 89-94.

Dow, W.G., 1974, Application of Oil-Correlation and Source-Rock Data to Exploration in Williston Basin, American Association of Petroleum Geologists Bulletin, v. 58, p. 1253-1262.

Egenhoff, S., Jaffri, A., Amrouni, K., & Newby, W., 2010, The Three Forks Formation – facies distribution and sequence architecture as a key to develop a new play in the Williston Basin of North Dakota and Montana, Final Report, Colorado State University, p. 2-25.

Egenhoff, S., Jaffri, A., & P., Medlock, 2011, Climate control on reservoir distribution in the Upper Devonian Three Forks Formation, North Dakota and Montana, Search and Discovery Article #50410, http://www.searchanddiscovery.com/abstracts/html/2011/annual/abstracts/Egenhoff2.html (accessed March 4 2013).

Egenhoff, S., Kolte, K., & Maletz, J., 2013, Petrology as a tool to delineate sweet spots the Middle Bakken reservoir of the Williston Basin in North Dakota and Montana, Progress report for Marathon Oil and Gas, Colorado State University, p. 2-53.

Geologic Atlas of the Rocky Mountain Region, 1972, Rocky Mountain Association of Geologists, Denver, Colorado, p. 81-184.

Gerhard, L.C., Anderson, S.B., Fischer, D.W., 1990, Petroleum Geology of the Williston Basin, In: Interior Cratonic Basins, M.W., Leighton, D.R., Kolata, D.F., Oltz, and J.J., Eidel, eds. American Association of Petroleum Geologists, Memoir 51, p. 507-559.

Goldstein, J.I., Newbury, D.E., Joy, D.C., Lyman, C.E., Echlin, P., Lifshin, E., Sawyer, L., and Michael, J.R., 2003, Scanning Electron Microscopy and X-Ray Microanalysis (third edition), New York, Kluwer Academic Plenum Publishers, 689 p.

Heck, T.J., LeFever, R.D., Fischer, D.W., and LeFever, J., 2002, Overview of the Petroleum Geology of the North Dakota Williston Basin: North Dakota Geological Survey, Bismark, ND, http://www.nd.gov/ndgs/Resources/WBPetroleumnew.asp (accessed March 13 2013).

Jacka, A.D., 1984, Intracrystalline porosity – a newly discovered pore type in dolostone reservoirs and implications for dedolomitization and pseudospiculites, American Association of Petroleum Geologists Bulletin, v. 68, 491 p.

Kent, D.M., and Christopher, J.E., 1994, Geological History of the Williston Basin and Sweetgrass Arch: In: Geological Atlas of the Western Canada Sedimentary Basin. Mossop, G.D., and Shetsen, I., eds. Canadian Society of Petroleum Geologists, p. 421-429.

LeFever, J.A., 2008, Isopachs of the Three Forks Formation, http://www.dmr.nd.gov/ndgs/Publication_List/pdf/geoinv/GI_64.pdf (accessed March 9 2014).

LeFever, J.A., LeFever, R.D., and Nordeng, S.H., 2011, Revised Nomenclature for the Bakken Formation (Mississippian-Devonian), North Dakota: Bakken Guidebook, Chapter 1. The Bakken-Three Forks Petroleum System in the Williston Basin, John W. Robinson, Julie

A. LeFever, Stephanie B. Gaswirth, eds. Denver, Colo.: Rocky Mountain Association of Geologists, p. 11-26.

Lexicon of Canadian Geologic Units, 2010, 'Three Forks Group'.

Lowe, D.R., 1975, Water escape structures in coarse-grained sediments, Sedimentology, v. 22, p. 157-204.

Lowe, D.R., 1976, Subaqueous liquified and fluidized sediment flows and their deposits, Sedimentology, v. 23, p. 285-308.

Nekhorosheva, V.V., 2011, Stratigraphy, Diagenesis and Fracture Characterization of the Three Forks Formation, Montana, Wyoming and South Dakota, Master's Thesis, Colorado School of Mines, Golden, Colorado, 204 p.

Nicholas, M.B.P., 2007, Devonian Three Forks Formation, Manitoba (NTS 62F parts of 62G, K): preliminary hydrocarbon and stratigraphic investigations; in Report of Activities 2007, Manitoba Science, Technology, Energy and Mines, Manitoba Geological Survey, p. 175-185.

Obermeier, S.F., 1996, Use of liquefaction-induced features for palaeoseismic analysis – an overview of how seismic liquefaction can be distinguished from other features and how their regional distribution and properties of source sediment can be used to infer the location and strength of Holocene-paleo-earthquakes, Engineering Geology v. 44, p. 1-76.

Patterson, R.J., and Kinsman, D.J.J., 1982, Formation of Diagenetic Dolomite in Coastal Sabkha Along Arabian (Persian) Gulf, American Association of Petroleum Geologists Bulletin, v. 66, 28 p.

Pitman, J. K., Price, L. C., and LeFever, J. A., 2001, Diagenesis and fracture development in the Bakken Formation, Williston Basin - implications for reservoir quality in the middle member, Version 1.0. Denver, Colo.: U.S. Dept. of the Interior, U.S. Geological Survey Professional Paper, 1653, 19 p.

Purser, B., Tucker, M., and Zanger, D., 1994, Dolomites: Special Publication, International Association of Sedimentology, v. 21, 464 p.

Smith, M.G., and Bustin, R.M., 2000, Late Devonian and Early Mississippian Bakken and Exshaw black shale source rocks, Western Canada Sedimentary Basin: A sequence stratigraphic interpretation, American Association of Petroleum Geologists Bulletin, v. 84, p. 940-960.

Sonnenberg, S.A., Gantyno, A., and Sarg, R., 2011, Petroleum Potential of the Upper Three Forks Formation, Williston Basin, USA, Search and Discovery Article #110153, http://www.searchanddiscovery.com/documents/2011/110153sonnenberg/ndx_sonnenberg.pdf (accessed March 12 2014).

Weyl, P.K., 1960, Porosity Through Dolomitization: Conservation-Of-Mass Requirements, Journal of Sedimentary Petrology, v. 30, p. 85-90.

Wilson, E.N., Hardie, L.A., and Phillips, O.M., 1990, Dolomitization front geometry, fluid flow patterns, and the origin of massive dolomite: the Triassic Latemar buildup, northern Italy, American Journal of Science, v. 290, p. 741-796.

APPENDIX I

Table 1: Well ID numbers along with their operators and names

Well ID	Operator Name	Well Name
1405	Gofor Oil Inc.	Catherine E Peck2
2602	PetroHunt L.L.C.	Charlson SWD 2
2828	Texaco Inc.	L.J. Hovde 1
3363	Texaco Inc.	C. Pederson NCT-1
12019	EOG Resources	Bures 1-17H
16089	Samson Resources	Nordstog 14-23-161-98H
16160	Hess Corporation	State of North Dakota 1-11H
16458	Petro Hunt L.L.C.	Willard Johnson Trust 24B-2-1H
16565	Hess Corporation	H.Bakken 12-07
16771	Hess Corporation	EN-Rudland-156-94- 3328 H-1
16841	Fidelity	Deadwood 43-28H
17015	Headington Oil Co.	Nesson State 42X-36
17023	Whiting O & G	Braaflat 11-11H
17513	Brigham O & G	Olson 10-15-1H
E069	Cenergy Incorporated	1-4 Williams
R658	Maxus Energy	Short Fee 1-17H

Table 2: Point-counting data of the Upper Three Forks thin sections in the study area

RecNo	Slide_No	X	Y	Facies	porosity	dolomite	dol_rhomb	zoned_dol	overgrowth	clear_dol	microdol	dol_tot	pyrite	anhydrite	Clay_matrix	mono_qtz	poly_qtz	muscovite	hm_other	plagioclase	microcline
1	1405-10822	-102.949065	47.78788	massive_bedded_dol	0.33	23.33	2	0.33	0.33	8.33	5.33	39.65	0.66	19	10.66	10.66	3	0	2.66	0	0
2	1405-10852.2	-102.949065	47.78788	intercalated_dol_mud	8.33	36.66	0.33	0.33	0	0	2.66	39.98	0.66	0	5	28.33	16.66	0.33	0	0.33	0.33
3	2602-9815.5	-102.941239	48.106547	intercalated_dol_mud	0.66	59.66	0	0	0.66	0	0	60.32	0.33	0.33	22	13	3.33	0	0	0	0
4	2602-9828.2	-102.941239	48.106547	intercalated_dol_mud	2.66	47	0	0	0.33	0	5.66	52.99	5	0	20	18.66	0.66	0	0	0	0
5	2602-9834.2	-102.941239	48.106547	monomict_cong	2	51.33	0	0	0.33	0	0	51.66	0.66	0	24.33	8	13.33	0	0	0	0
6	2828-11142.2	-103.277684	48.167336	intercalated_dol_mud	8.66	31.66	0	0	0	0	47	78.66	1.66	0	11	0	0	0	0	0	0
7	2828-11166	-103.277684	48.167336	monomict_cong	6	50.33	0	0	0.66	0	0	50.99	0	2	5	20	16	0	0	0.33	0
8	3363-10222.9	-103.132321	48.406909	massive_bedded_dol	6.66	62	0	0	0	0	3.33	65.33	0.66	0.66	0	15.66	9.66	0	0.66	0.66	0
9	3363-10233.5	-103.132321	48.406909	intercalated_dol_mud	6.66	37	4	0	0	0.33	9.66	50.99	11.66	0	13	5	0	0	0	0	0
10	3363-10236.5	-103.132321	48.406909	intercalated_dol_mud	6.66	33.66	3.33	0	0	0	22.66	59.65	3.66	0	6.66	18.66	2	1.33	0	0	1.33
11	12019-10609.8	-101.002024	48.880675	intercalated_dol_mud	1.33	53	0	0	1.33	0	0	54.33	0.33	0.33	27.33	10.33	5.66	0	0	0	0
12	12019-10611.7	-101.002024	48.880675	intercalated_dol_mud	1.33	38.66	0	0.66	1	0	3.33	42.65	3.66	0.33	36.66	13	1.33	0	0	0	0
13	16089-8714	-103.3579341	48.76456428	intercalated_dol_mud	10.33	19	5.33	2.33	0.66	1.33	21	49.65	4.66	0.33	22.66	10.33	1	1	0	0	0
14	16089-8725.2	-103.3579341	48.76456428	intercalated_dol_mud	10.33	43.66	0	2.66	1.33	0	0	47.65	7	5.33	1.66	17	6.33	1.33	1.66	1.66	0
15	16089-8729.4	-103.3579341	48.76456428	monomict_cong	11.66	42.66	0	5.66	0	0	6.66	54.98	1.66	0	8.66	18.66	1.66	2.66	0	0	0
16	16160-9543.3	-102.6663559	48.53077511	intercalated_dol_mud	0.33	65.66	0	0	0	0	0.33	65.99	0.33	0	10	13	10.33	0	0	0	0
17	16160-9560.2	-102.6663559	48.53077511	massive_bedded_dol	0	62	0	0	0	0	0	62	0	0.66	3.33	18	15	0	0.66	0.33	0
18	16160-9565.3	-102.6663559	48.53077511	monomict_cong	2	50	0	0	0.33	0	0	50.33	1.33	0	5.66	31.66	7.33	0.33	0	0.66	0
19	16458-9219.4	-103.4262395	48.67496022	intercalated_dol_mud	3.66	21	3	3.33	0.33	0	30.33	57.99	5.33	0.33	7.33	23	2	0.33	0	0	0
20	16458-9235.7	-103.4262395	48.67496022	massive_bedded_dol	6.66	37.66	8	5.33	0.66	0	2	53.65	0	1.33	0	31	6.66	0	0	0	0
21	16458-9241	-103.4262395	48.67496022	monomict_cong	8	25	10.33	4	0.33	0	4.33	43.99	3.66	0	12	27	5	0	0.33	0	0
22	16565-9728.4	-102.9058076	48.4374946	intercalated_dol_mud	8.66	25	11.33	3.66	3	0	12.66	55.65	3	0	23.66	8.66	0	0	0	0	0
23	16565-9743.6	-102.9058076	48.4374946	monomict_cong	9.66	32.33	11.33	3.33	1	0	0.66	48.65	1.33	0	14.33	25	0.66	0	0.33	0	0
24	16771-10421.8	-102.7764384	48.2850898	intercalated_dol_mud	5	19.66	12	7	3.66	0	9	51.32	5.33	0	26.33	10.66	1.33	0	0	0	0
25	16771-10436a	-102.7764384	48.2850898	intercalated_dol_mud	6.33	39.66	11.33	2.66	1.66	0	6.66	61.97	2.66	0	4.66	22.66	1.66	0	0	0	0
26	16771-10436b	-102.7764384	48.2850898	intercalated_dol_mud	6.33	19.66	7	4	3	0	0.33	33.99	4.33	0	1.66	38.33	15.33	0	0	0	0
27	16841-10206	-102.5049103	48.12913862	intercalated_silt_mud	0.66	61.33	0	0	0.33	0	0.66	62.32	0.66	0	10	17.66	9	0	0	0	0
28	16841-10222	-102.5049103	48.12913862	massive_bedded_dol	8	50.33	0	0	0	0	0	50.33	0	0.66	13.66	19.66	7.66	0	0.33	0	0
29	17015-10438.6	-102.8284633	48.29136544	intercalated_dol_mud	0.33	59.66	0	0	0.66	0	1.33	61.65	0	0	21.66	12.66	3.66	0	0	0	0
30	17015-10444.8	-102.8284633	48.29136544	intercalated_dol_mud	1	41	0	0	0	0	20	61	3.66		22.33	11.33	0.66	0	0	0	0
31	17015-10463.7	-102.8284633	48.29136544	intercalated_dol_mud	2.33	50	0	0	0.33	0	8.33	58.66	3.33	0.66	2.33	24.33	8.33	0	0	0	0
32	17023-9991	-102.3507478	48.09489323	intercalated_dol_mud	1.66	47.33	0	0	1	0	0	48.33	0	0	4.33	21.66	23.66	0	0	0	0
33	17023-9999.5	-102.3507478	48.09489323	intercalated_dol_mud	3	55	0	0	0	0	0.33	55.33	1.66	1	19.33	10.33	9.66	0	0	0	0
34	17023-10003.9	-102.3507478	48.09489323	monomict_cong	4.33	38.33	0	0	0	0	19.66	57.99	10.33		11.66	13.33	2.33	0	0	0	0
35	17513-10692.4	-103.7967746	48.18273996	massive_bedded_dol	1	55	0	0	2.33	0	0	57.33	0.66	9.33	5.33	11	15	0	0	0.33	0
36	17513-10696.3	-103.7967746	48.18273996	monomict_cong	5.33	40	0	0	0.33	0	11.66	51.99	19.33	0.33	16	5.33	1.66	0	0	0	0
37	E069-10073.2	-104.671156	47.788343	intercalated_dol_mud	6.33	25.66	2.33	0.33	0.33	4.33	28.66	61.64	5	0	23.33	3.33	0	0.33	0	0	0
38	E069-10077.2	-104.671156	47.788343	intercalated_dol_mud	9.33	31.66	31.66	10	0.33	0	1.33	74.98	1	0.33	10.66	28	6	0	0	0.66	0
39	R658-10489	-103.588055	47.149989	intercalated_dol_mud	12.66	27	8	0.66	2	0	2	39.66	2	0	27	16.66	0	0.66	0.66	0	0
40	R658-10489.1	-103.588055	47.149989	intercalated_dol_mud	3.66	21	2.33	0	0.33	0	7.33	30.99	4.33	0	13.33	40.33	7	0	0	0.66	0
41	R658-10502	-103.588055	47.149989	intercalated_dol_mud	6	51	2.66	2	0	0	0	55.66	3.33	0	13.33	14.33	6.66	0	0.66	0	0
42	R658-10517	-103.588055	47.149989	intercalated_dol_mud	6.33	38.33	4.66	2	1.66	0	1.33	47.98	1.33	1.33	2.66	27	12.33	0.33	0.66	0	0

Table 3: Electron Microprobe Values of thin-section number 12019-10609.3

C:\UserData\Egenhoff\CSU_2013-05-17.MDB											
Probe User											
USGS Denver											
Electron Microbeam Laboratory											
Nominal Beam: 1											
SAMPLE	LINE	TOTAL	FeO WT%	MnO WT%	BaO WT%	MgO WT%	CaO WT%	SO3 WT%	SrO WT%	SiO2 WT%	CO2 WT%
Un 7 12019-10609.3	98	100	0.2	0.15	0.14	20.7	31.8	0.05	0.00	0.17	46.8
Un 7 12019-10609.3	99	100	0.5	0.07	0.04	21.2	31.7	0.01	0.01	1.27	45.3
Un 7 12019-10609.3	100	100	0.4	0.00	0.15	21.6	32.4	0.10	0.04	0.70	44.6
Un 7 12019-10609.3	101	100	0.2	0.03	0.02	21.2	32.6	0.15	0.07	1.09	44.7
Un 7 12019-10609.3	102	100	0.9	0.60	0.03	21.0	32.0	0.09	0.00	0.68	44.7
Un 7 12019-10609.3	103	100	1.3	0.65	0.00	22.1	34.6	0.04	0.00	0.09	41.3
Un 7 12019-10609.3	104	100	11.8	0.69	0.00	14.3	31.1	0.00	0.00	0.10	41.9
Un 7 12019-10609.3	105	100	11.3	0.35	0.00	12.5	27.5	0.11	0.01	0.12	48.2
Un 7 12019-10609.3	106	100	10.4	0.59	0.00	14.5	31.4	0.02	0.00	0.10	42.9
Un 7 12019-10609.3	107	100	12.6	0.62	0.12	13.5	31.5	0.08	0.01	0.25	41.3
Un 7 12019-10609.3	108	100	12.0	0.73	0.00	13.4	30.4	0.03	0.01	0.15	43.2
Un 7 12019-10609.3	109	100	11.7	0.63	0.17	14.1	31.7	0.07	0.02	0.07	41.5
Un 7 12019-10609.3	110	100	9.9	0.49	0.00	15.9	33.8	0.00	0.04	0.12	39.8

APPENDIX II

SEDIMENTOLOGY

A. Lithological Description of Cores

The sedimentological observations summed up in this thesis are exclusively built on macroscopical observations from 16 cores of the upper Three Forks Formation (cf. Berwick, 2008; Egenhoff et al., 2011; Nekhorosheva, 2011; Sonnenberg et al., 2011). One distinct facies (F 1) and two facies associations (FAs) can be differentiated in this succession (Berwick 2009; Egenhoff et al. 2011): F 1 is composed of monomict clast-supported conglomerate, FA 1 consists of bedded to massive dolomites and FA 2 shows intercalated dolomites with clay-rich siliciclastic mudstones.

The monomict clast-supported conglomerate (F 1) is characterized by light pink to tan colored dolomite clasts that may or may not be supported by clay matrix. The dolomite clasts range in size from 0.5 to 2.5 cm. These clasts are either randomly oriented or at places may be preferentially aligned. The clay matrix in this facies is rarely present. This facies lacks distinct sedimentary structures.

The bedded to massive dolomites (FA 1) are characterized by thickly bedded and massive homogenous dolomite beds. These beds range in thickness from 1 to 3 ft. This facies association mostly lacks clearly visible sedimentary structures but rarely may exhibit faint laminations. The thickness of this facies association can be up to 3 ft (0.9 m). It appears tan to pinkish in color.

The intercalated dolomites with clay-rich siliciclastic mudstones (FA 2) are characterized by beds of greenish clay-rich mudstone and light pink to tan-colored dolomites. However, the proportions of these two lithologies changes from core to core, though in places comprising approximately fifty percent of each lithology. The tan-colored dolomite is slightly more

abundant in the lower part of the upper Three Forks cores while the clay-rich mudstone increases in the upper portion of the cores. The beds vary in thickness from 0.25 to 1 ft (0.07 to 0.3 m). The dolomite beds appear in various forms such as massive, brecciated, flaser/lenticular bedded, and ripple-bedded. Subrounded to subangular clay rip-up clasts, disrupted clay laminae, disorganized clayey material, dolomite subangular clasts, pyrite nodules and anhydrite nodules occur within these light pink to tan colored dolomite beds. The pyrite and anhydrite nodules can be up to 5 cm in diameter. Other structures observed in these beds are clastic dykes, ball-and-pillow structures, slumps, convolute bedding, small scale reverse faults, flow folds, and scourmarks. The green clay-rich mudstone beds appear mostly uniformly massive but rarely may exhibit very faint laminations. Some of the mudstone beds may also show presence of dark colored clay clasts and light pink to tan colored dolomitic clasts. Like the dolomite beds, these mudstone beds also exhibit soft sediment deformation structures along with syneresis cracks.

The upper Three Forks Formation in general shows three forms/types of overall grain-size trends: either the sections exhibit one or two well-pronounced fining-upwards as e.g. section 2602 PetroHunt L.L.C. Charlson SWD 2 (Figure 12), they may show a fining-upward overlain by a coarsening-upward e.g. section 3363 Texaco Inc. C. Pederson NCT-1 (Figure 14), or they are devoid of any unequivocal overall grain-size trends e.g. section 12019 EOG Resources Bures 1-17 H (Figure 15). Of these 3 types, the overall fining-upward pattern is by far the most frequent and characterizes nine out of the sixteen sections.

B. Facies and Facies Association Interpretation

The presence of deformed dolomitic clasts in F 1 suggests that these clasts were only partly lithified and their preferential alignment may be indicative of a physical shock on these sediments during deposition. The sparse presence of clay surrounding the dolomite clasts can be attributed either to a physical shock these sediments experienced during deposition or to high energy currents that are responsible for the selective removal of clay surrounding the dolomite clasts. Hence, these dolomite clasts imply bed load transportation in aqueous and subaqueous environment suggesting prevalent high energy conditions.

The thick-bedded to massive dolomite in FA 1 indicates deposition from relatively high energy conditions. This thickly bedded to massive dolomite with very faint to completely absent laminations/structures may have been deposited either due to rapid deposition resulting in homogeneous sediment or it may also arise due to liquefaction implying sudden physical shock by earthquakes.

The intercalated beds in FA 2 suggest deposition under varying energy conditions. The light pink to tan colored dolomite is a result of bed load transport sedimentation in a high energy environment while the siliciclastic clay-rich green mudstones are a result of suspension settling in relatively low energy conditions (Egenhoff et al., 2010). The generally massive nature and the very faint laminations in clay-rich green mudstones suggest settling from suspension. The synsedimentary deformation structures in this facies association reflect the physical shock such as liquefaction that these sediments experienced (Lowe 1975, 1976; Obermeier 1996) shortly after deposition. The random orientation of broken dolomitic clasts and mud rip up clasts indicate erosive actions during high energy conditions.

Legend

Sedimentary Structures:

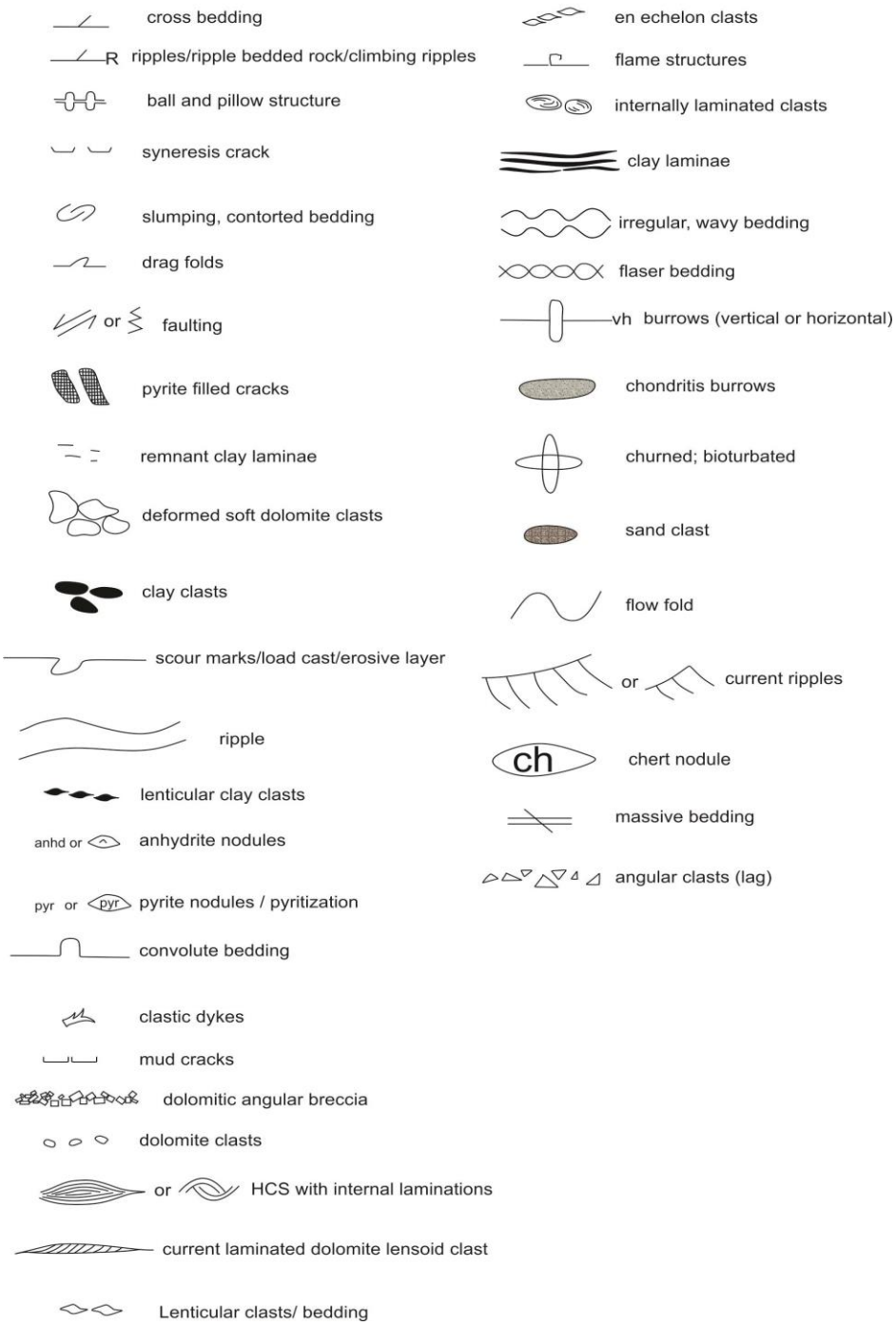

Figure 10: Key to all figures within the following appendices

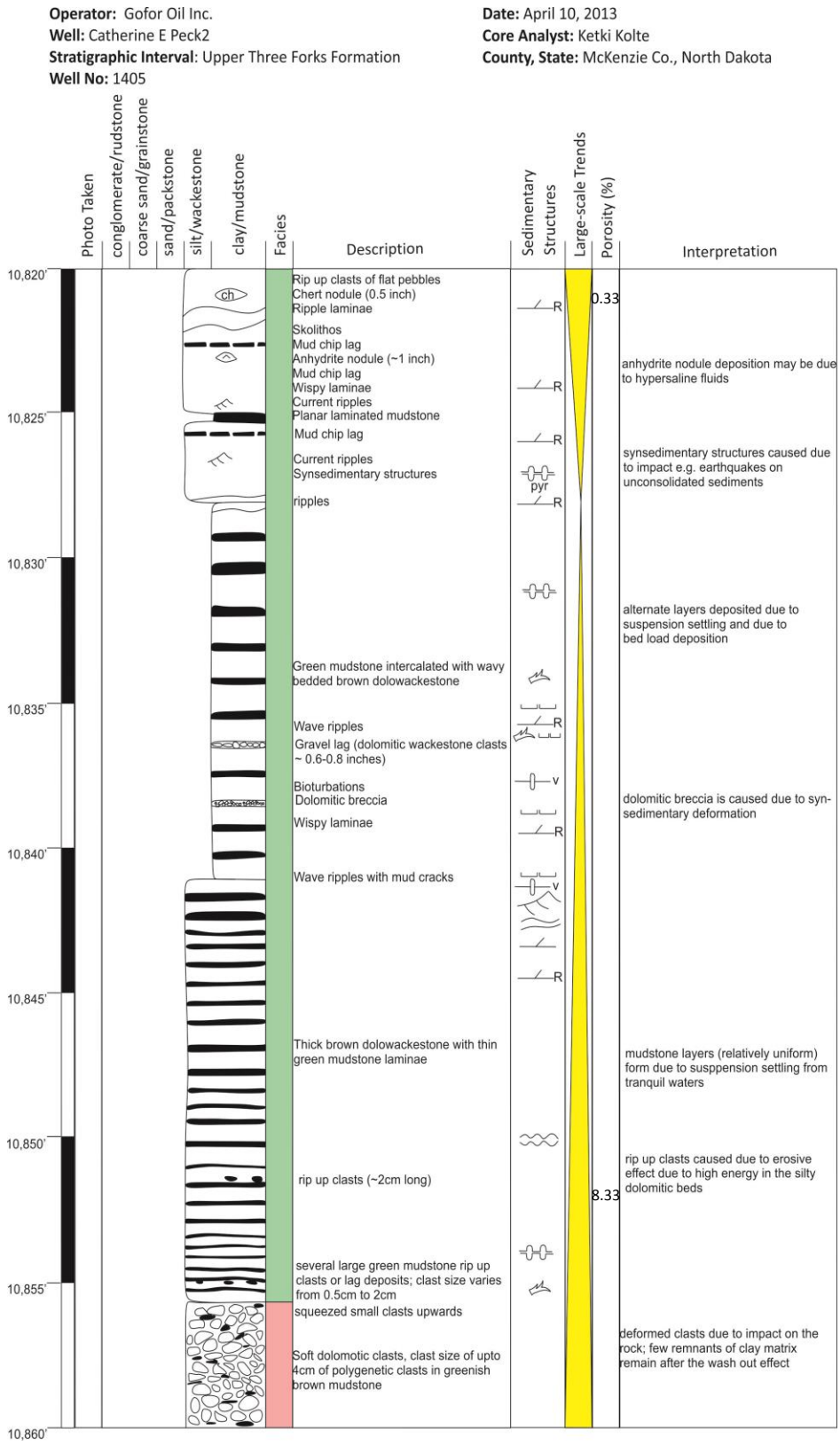

Figure 11: Stratigraphic description of Core #1405

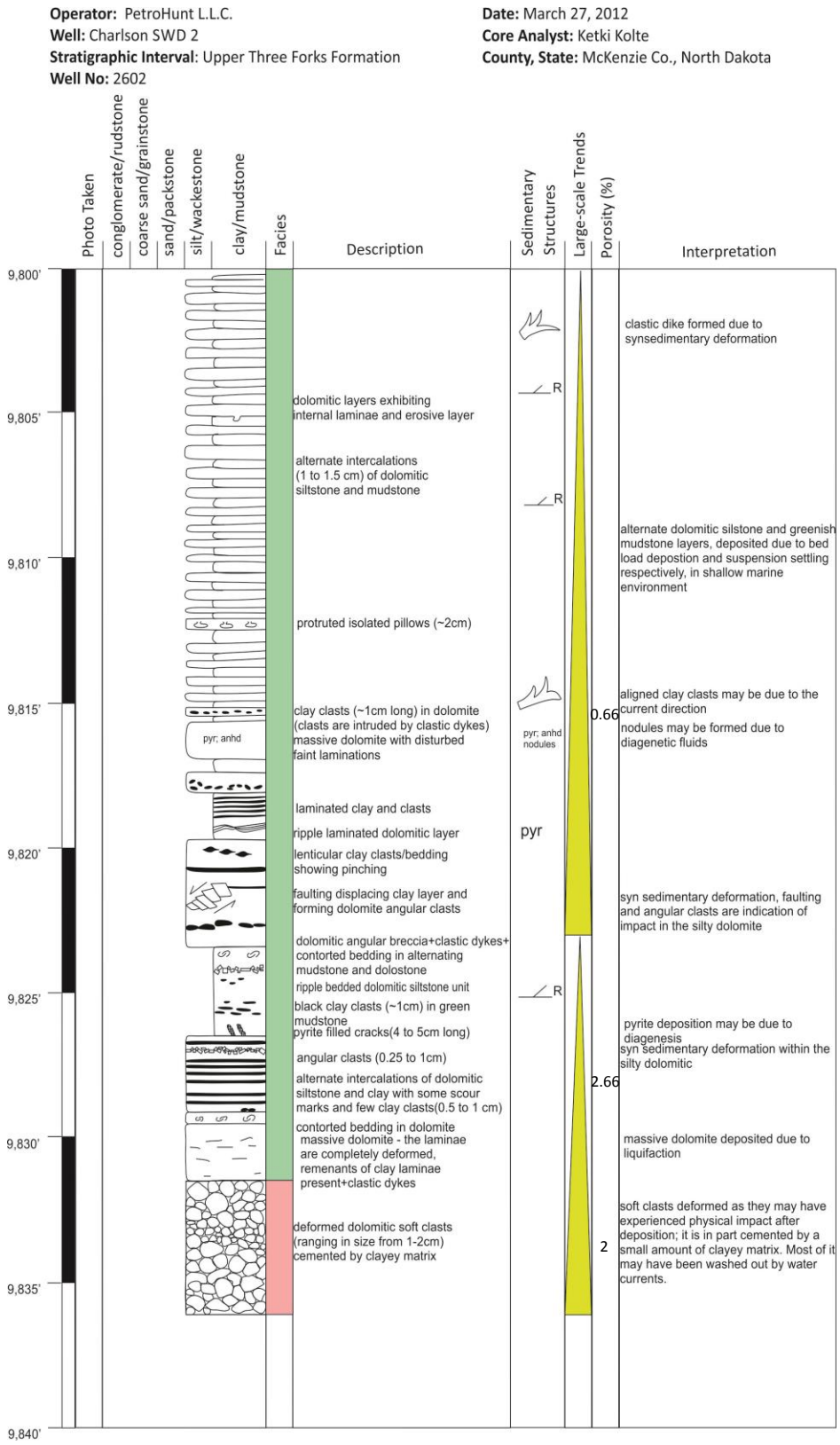

Figure 12: Stratigraphic description of Core #2602

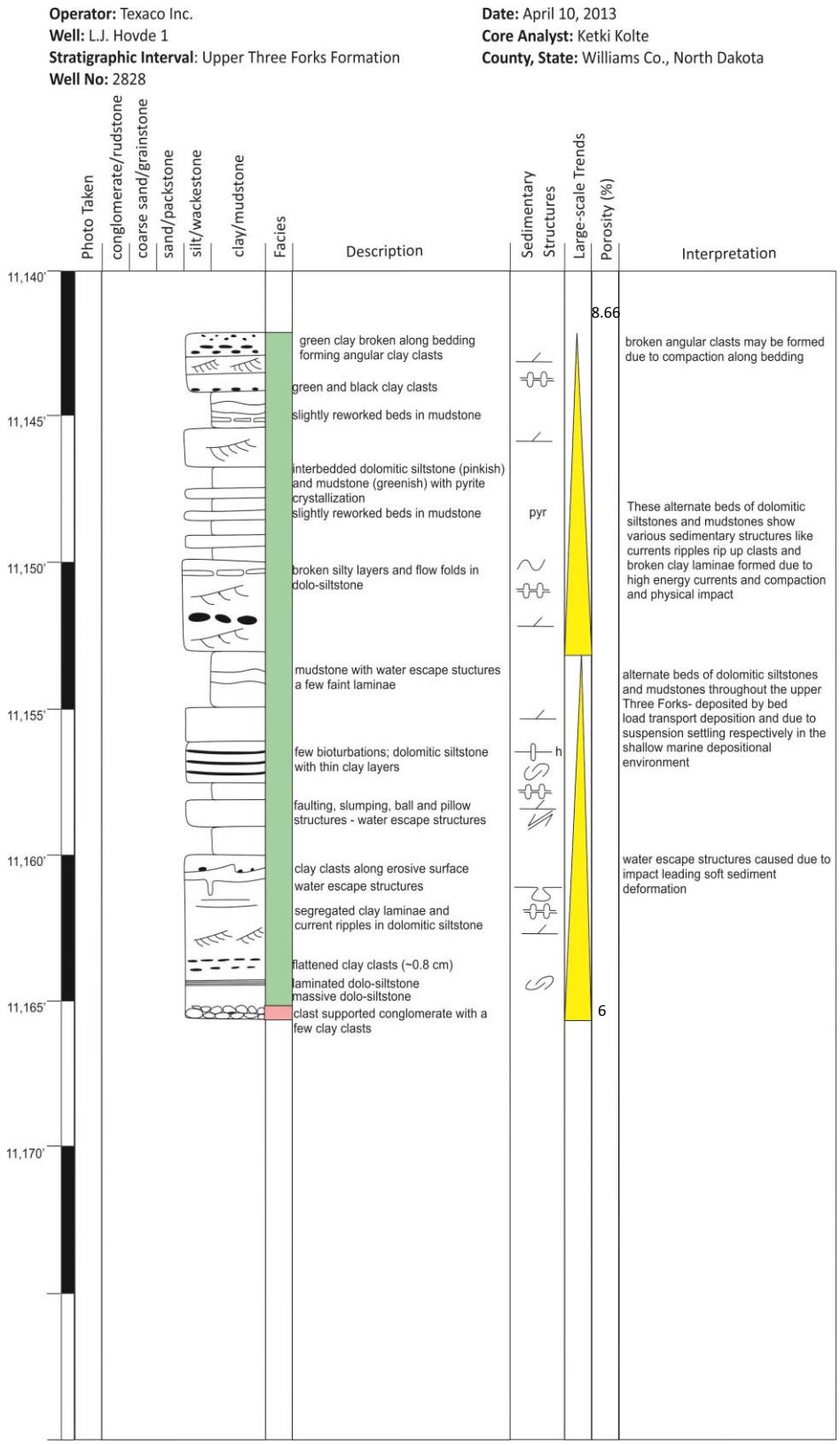

Figure 13: Stratigraphic description of Core #2828

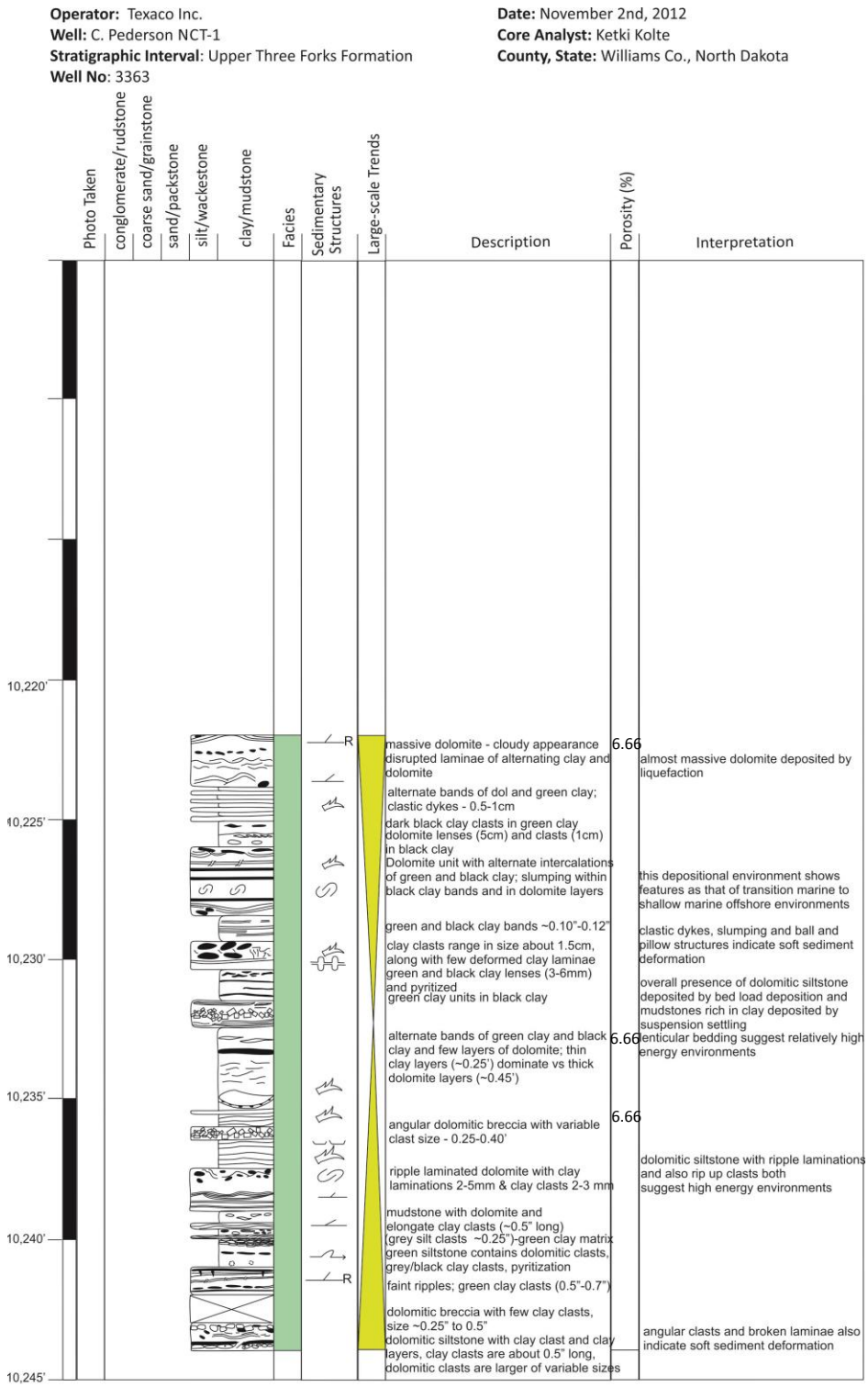

Figure 14: Stratigraphic description of Core #3363

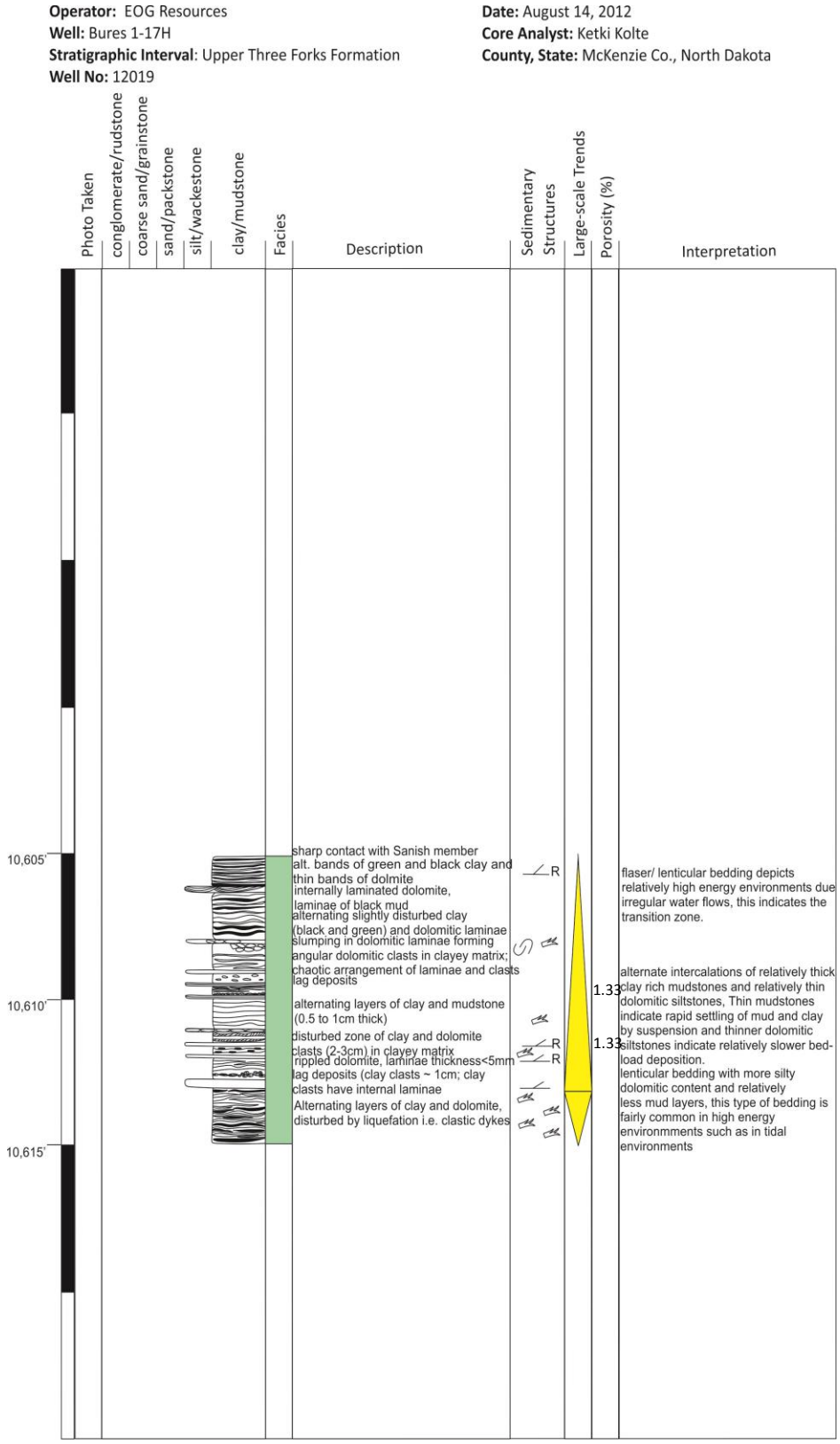

Figure 15: Stratigraphic description of Core #12019

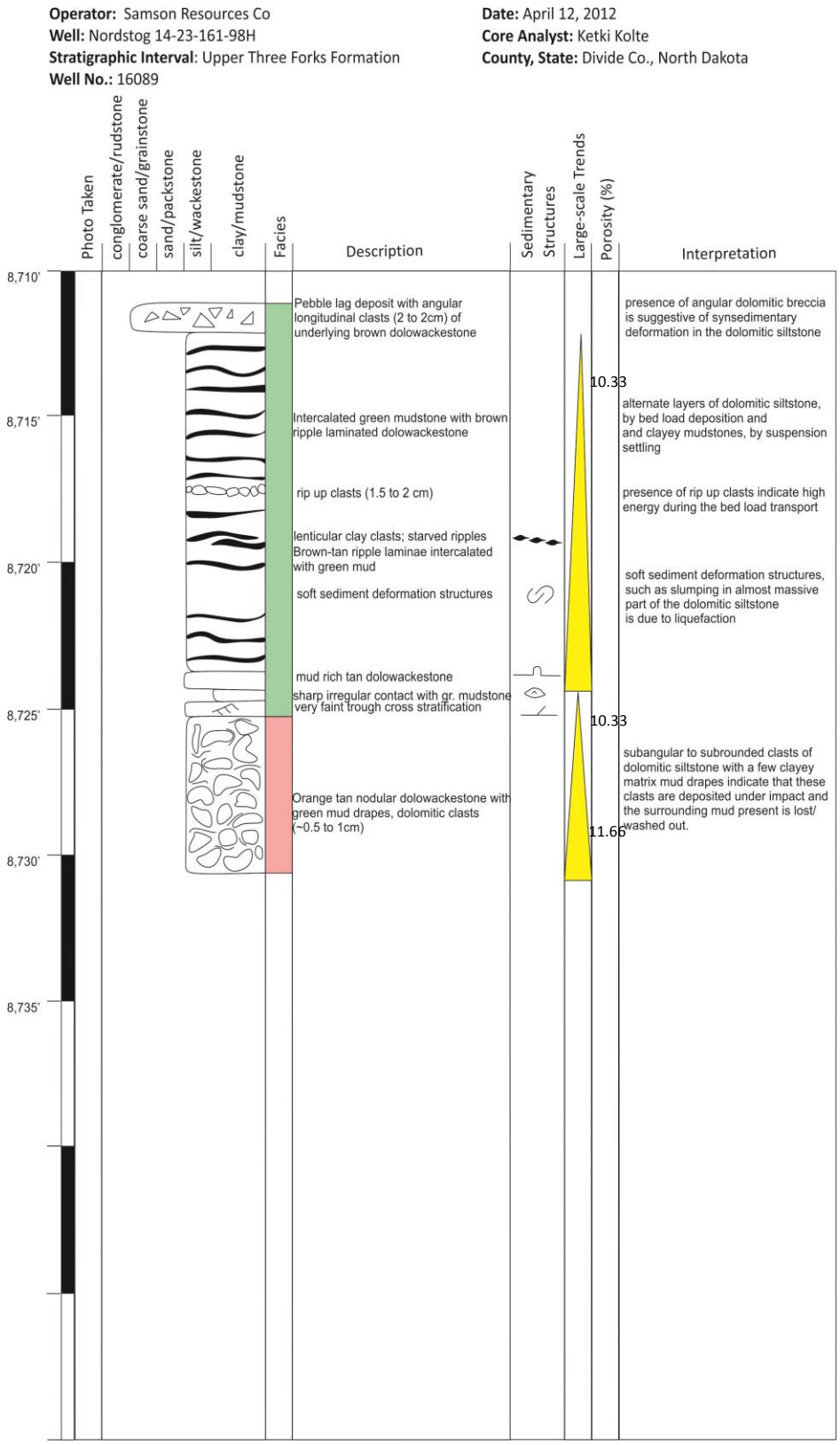

Figure 16: Stratigraphic description of Core #16089

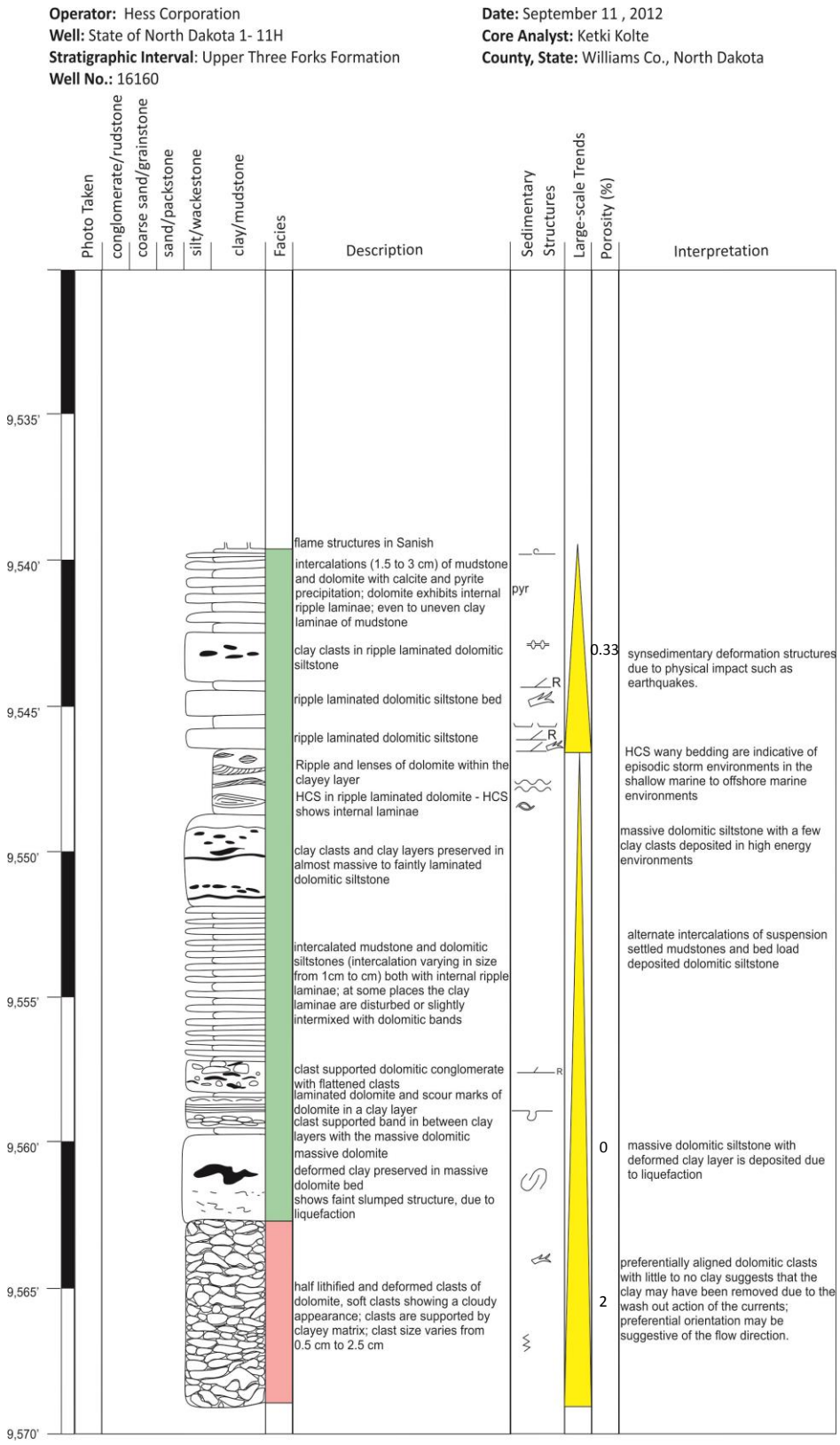

Figure 17: Stratigraphic description of Core #16160

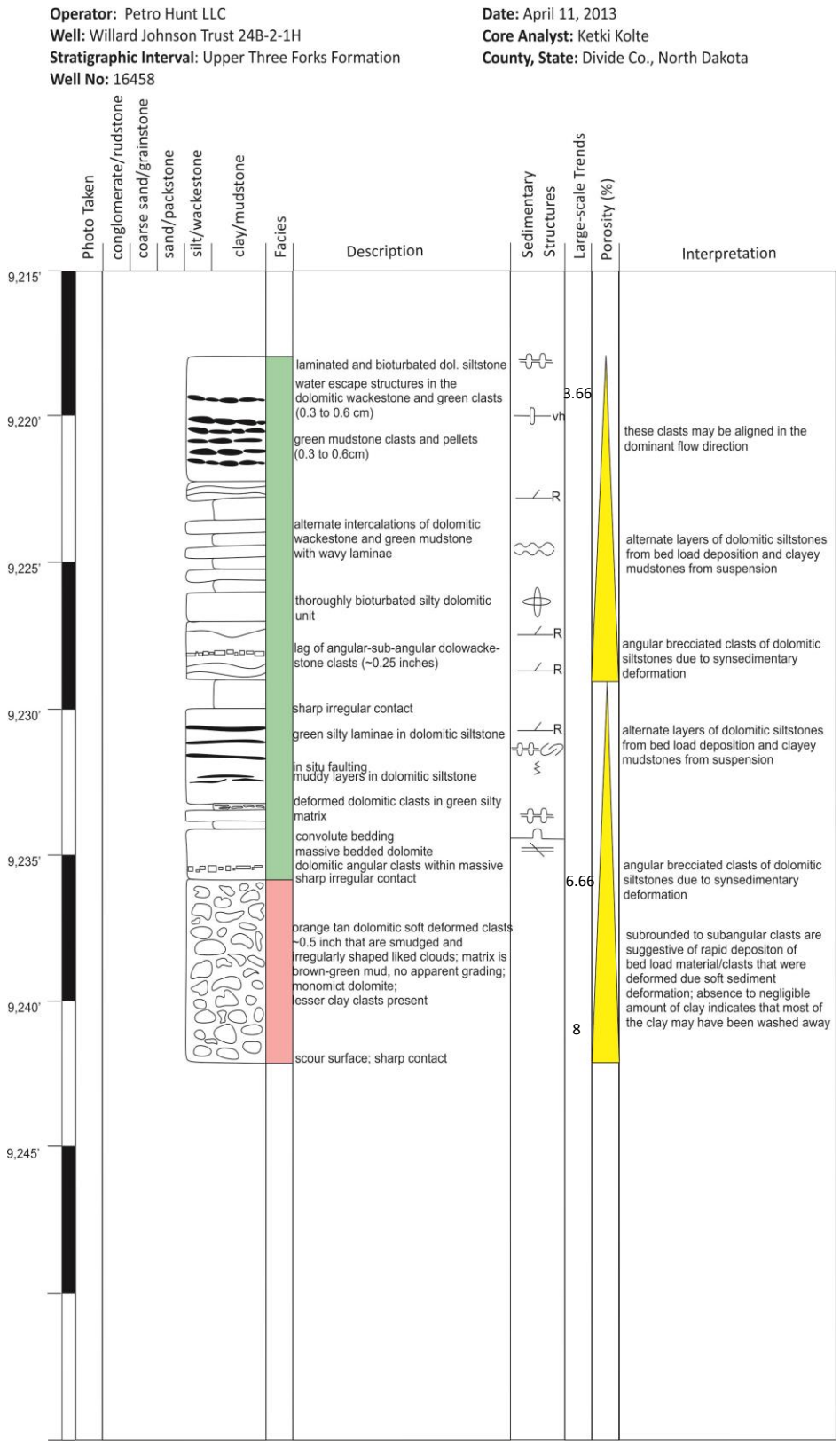

Figure 18: Stratigraphic description of Core #16458

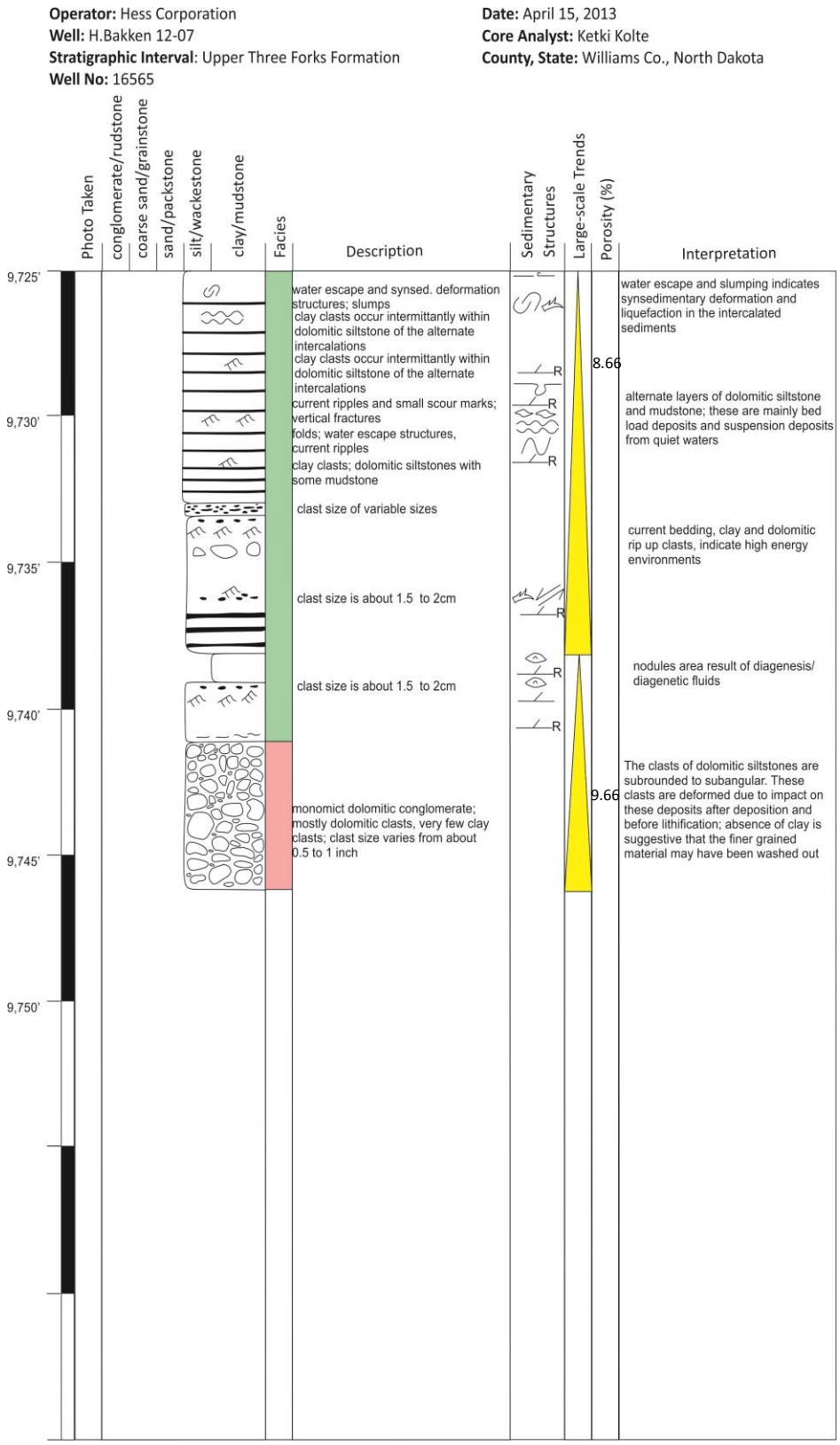

Figure 19: Stratigraphic description of Core #16565

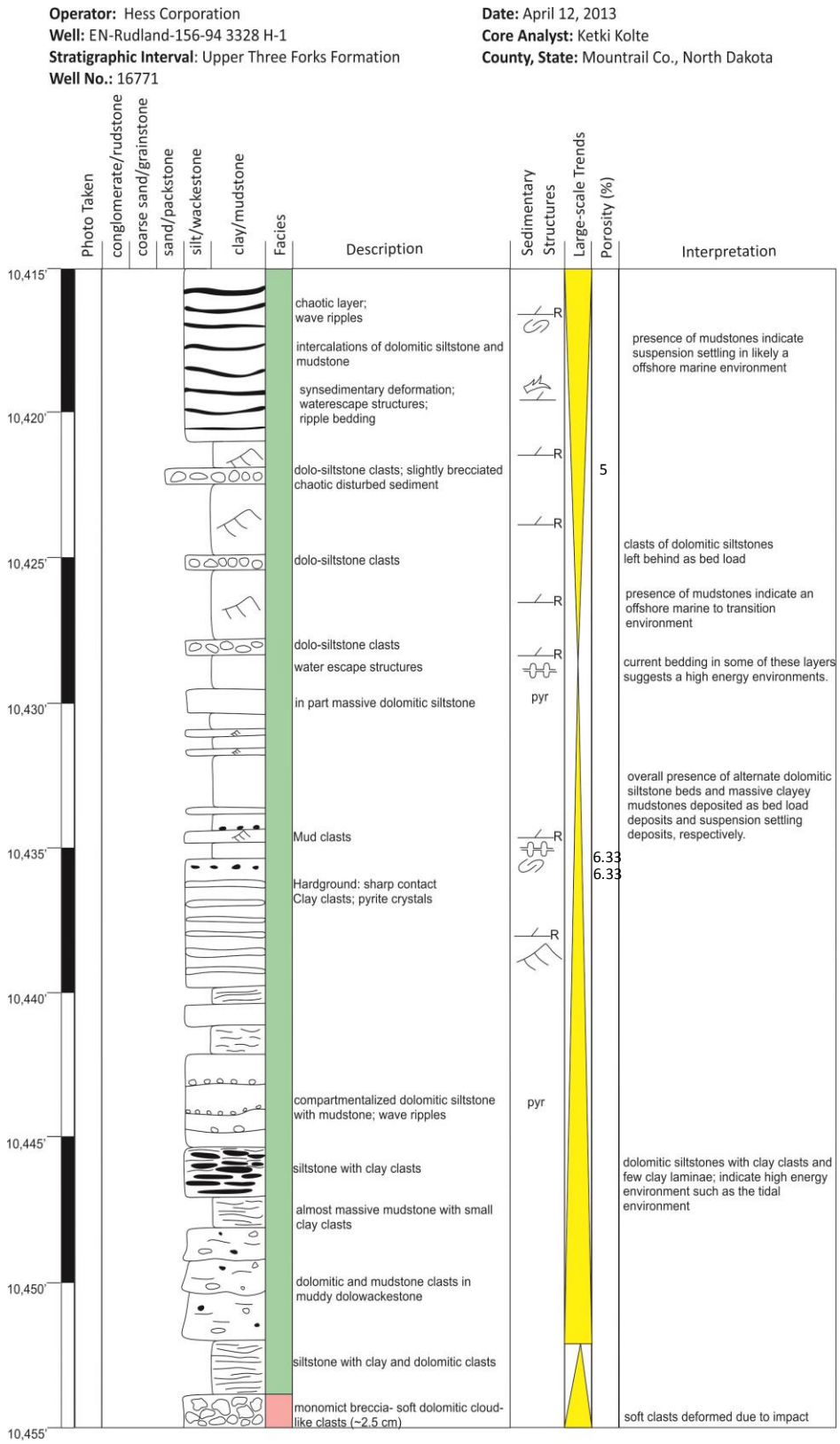

Figure 20: Stratigraphic description of Core #16771

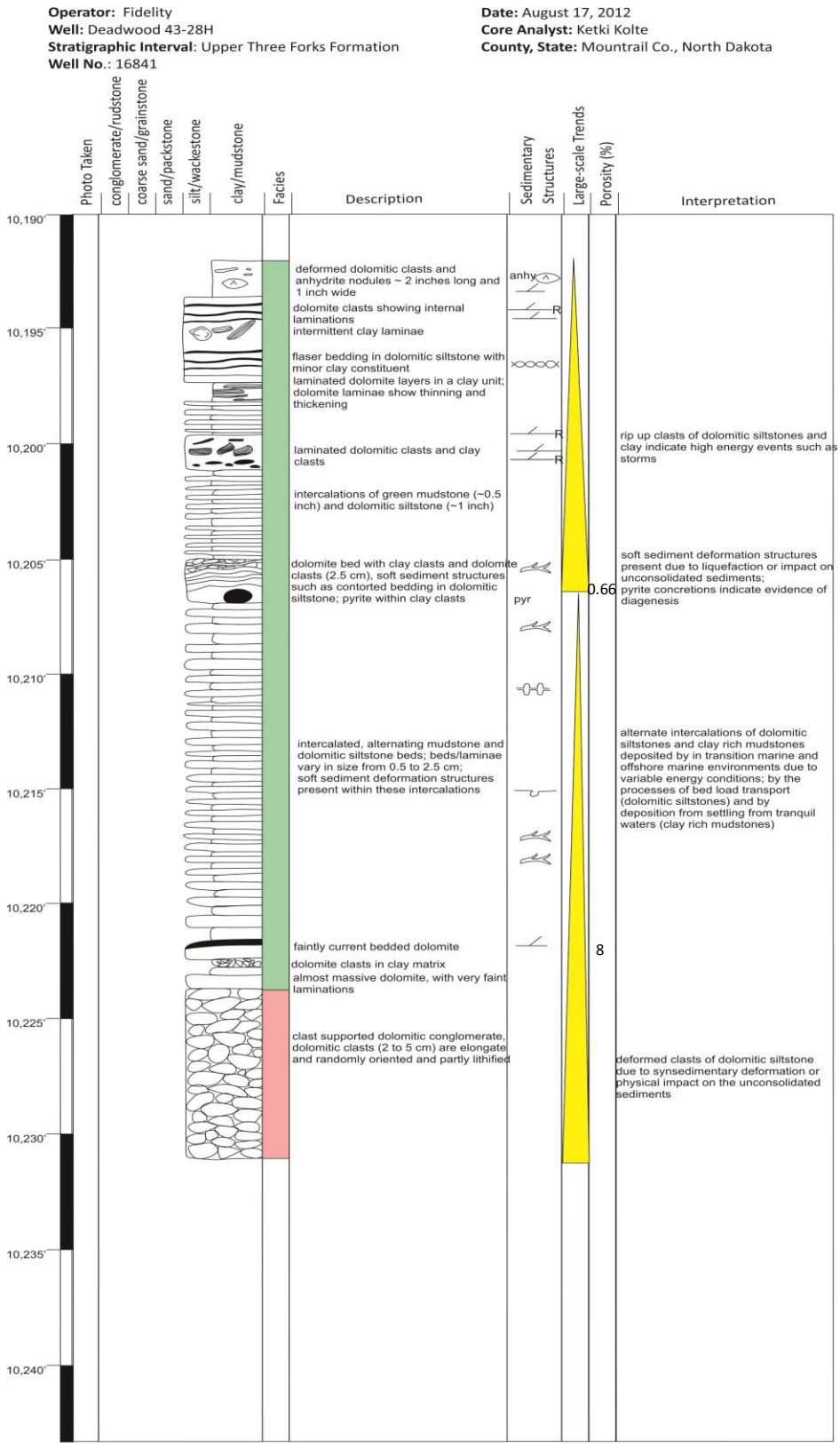

Figure 21: Stratigraphic description of Core #16841

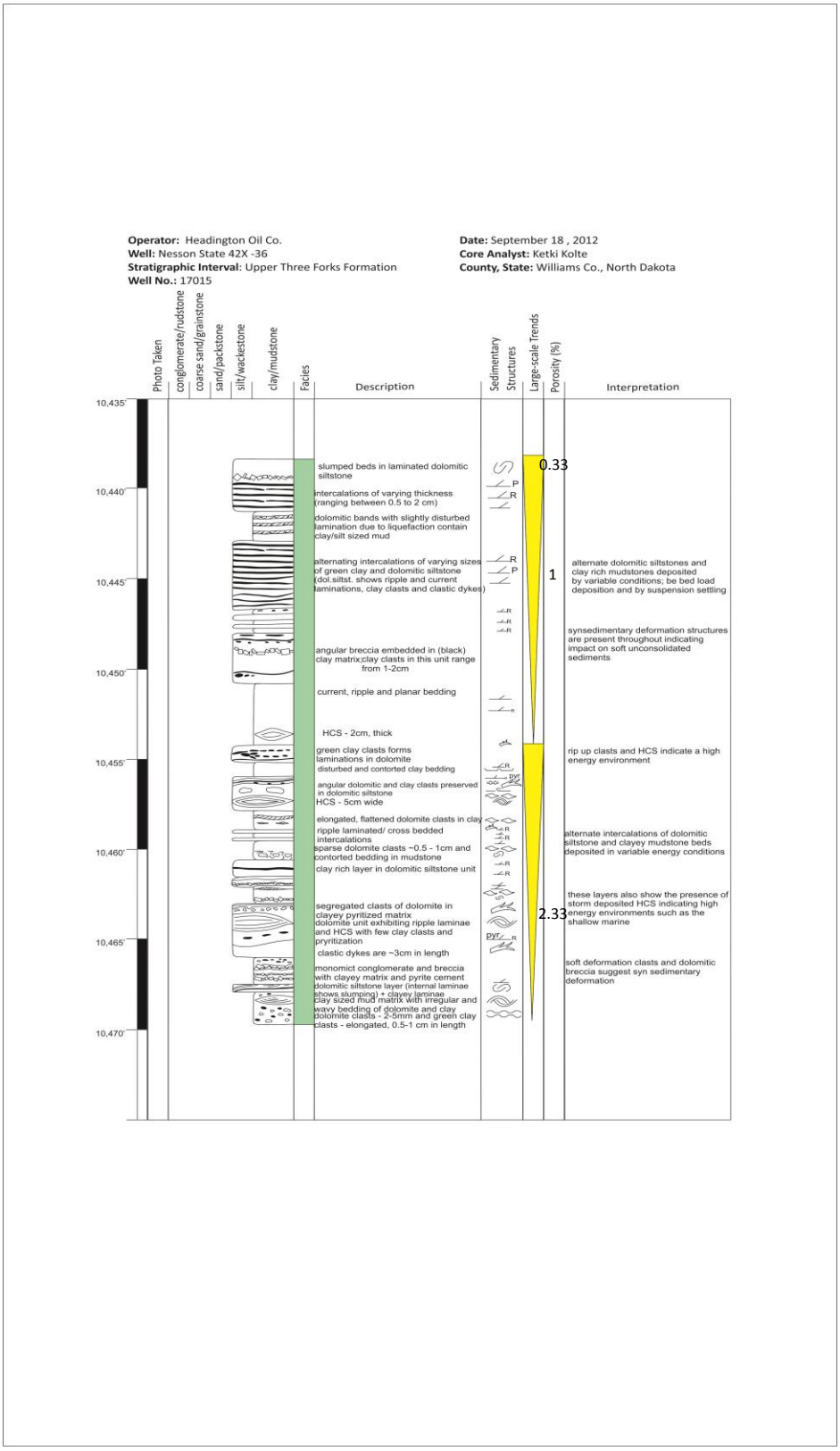

Figure 22: Stratigraphic description of Core #17015

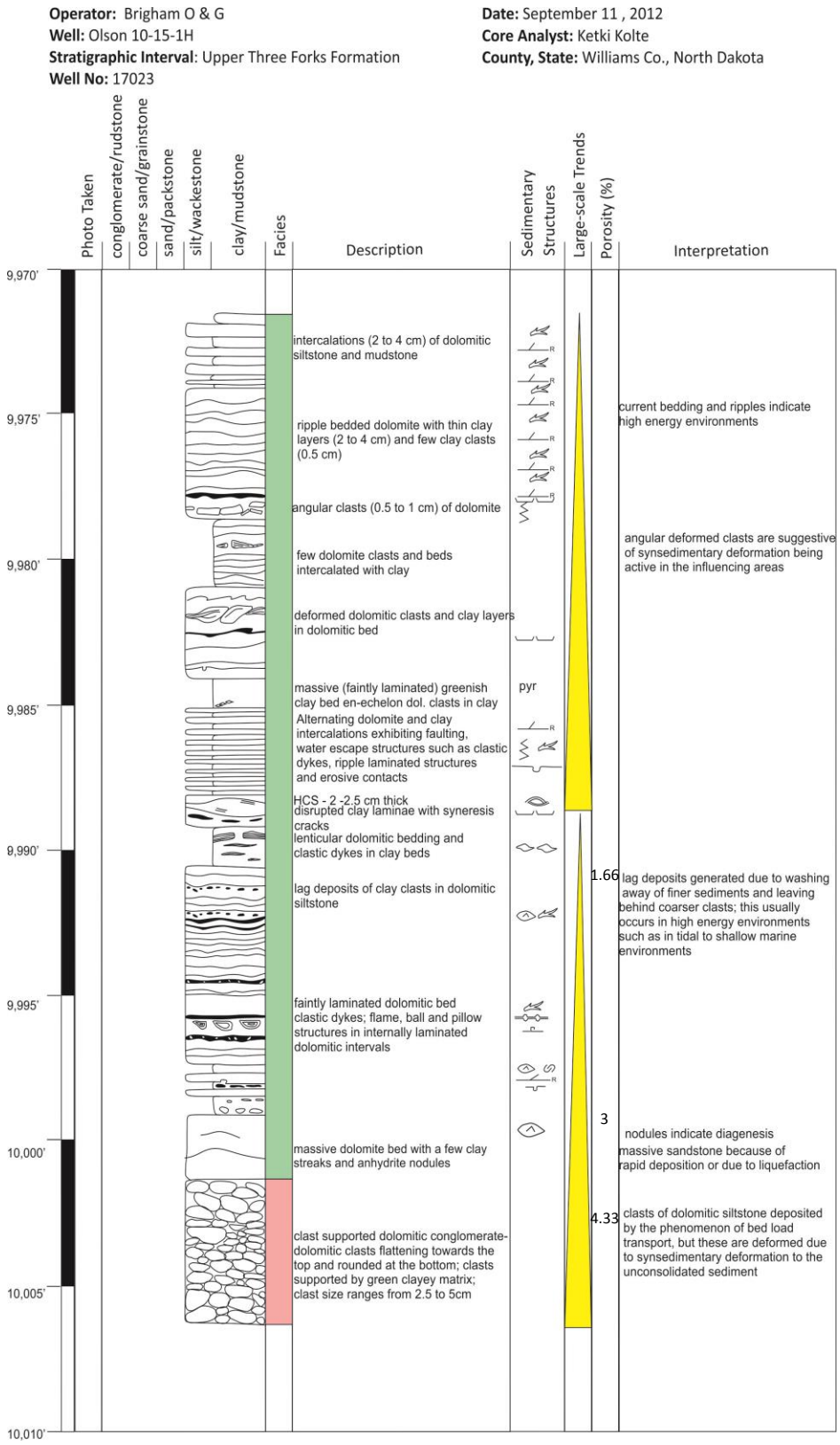

Figure 23: Stratigraphic description of Core #17023

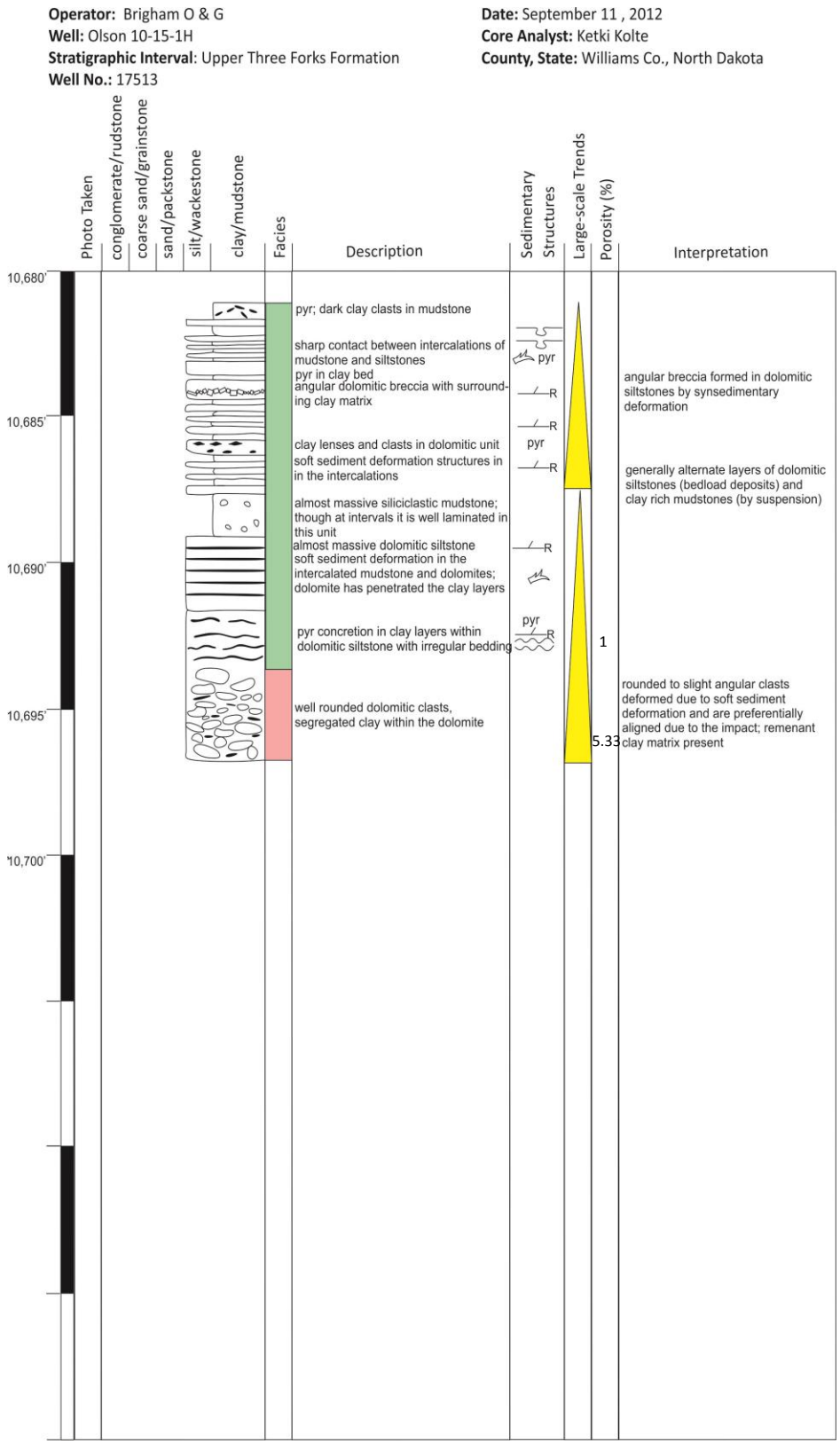

Figure 24: Stratigraphic description of Core #17513

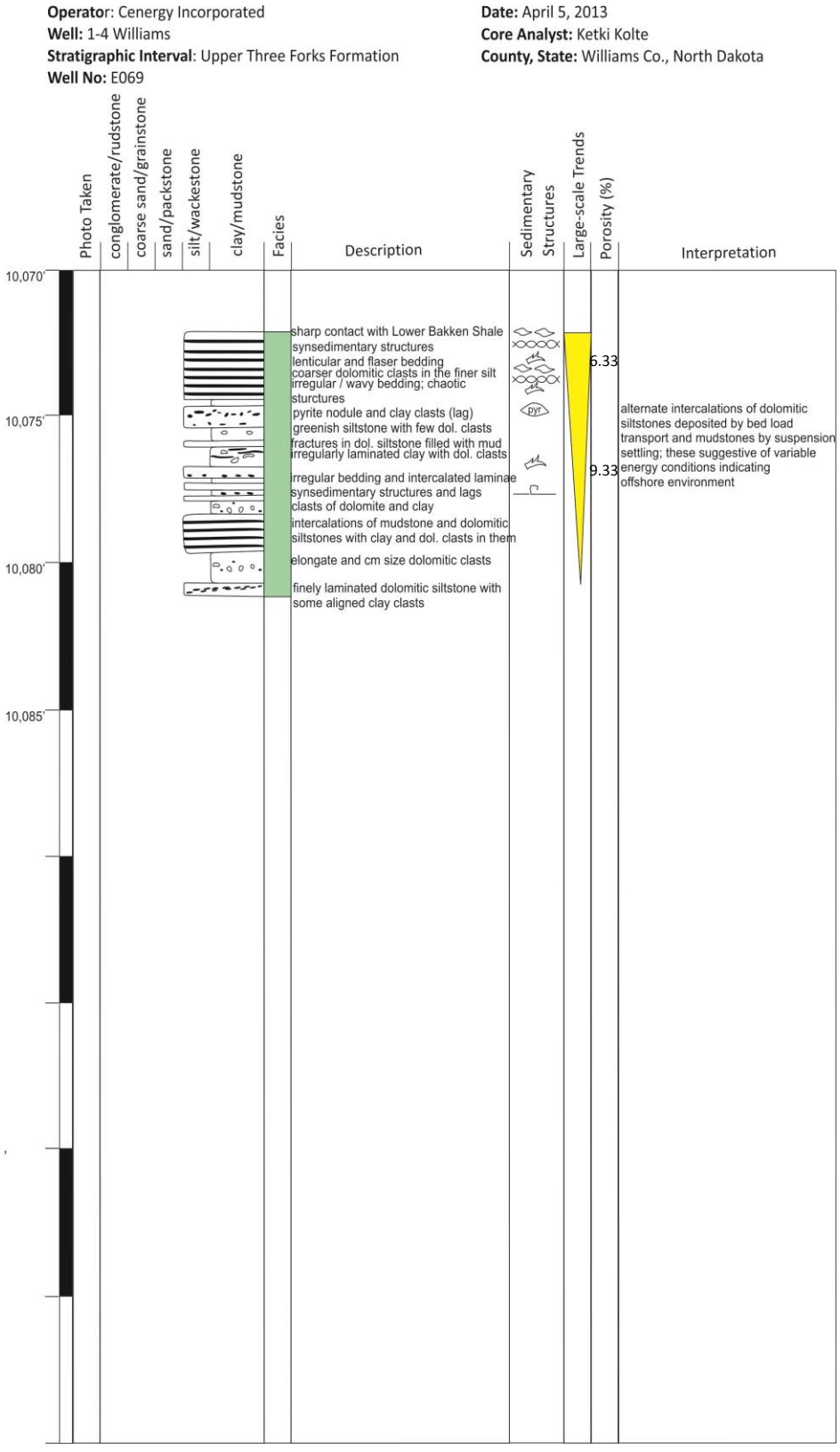

Figure 25: Stratigraphic description of Core #E069

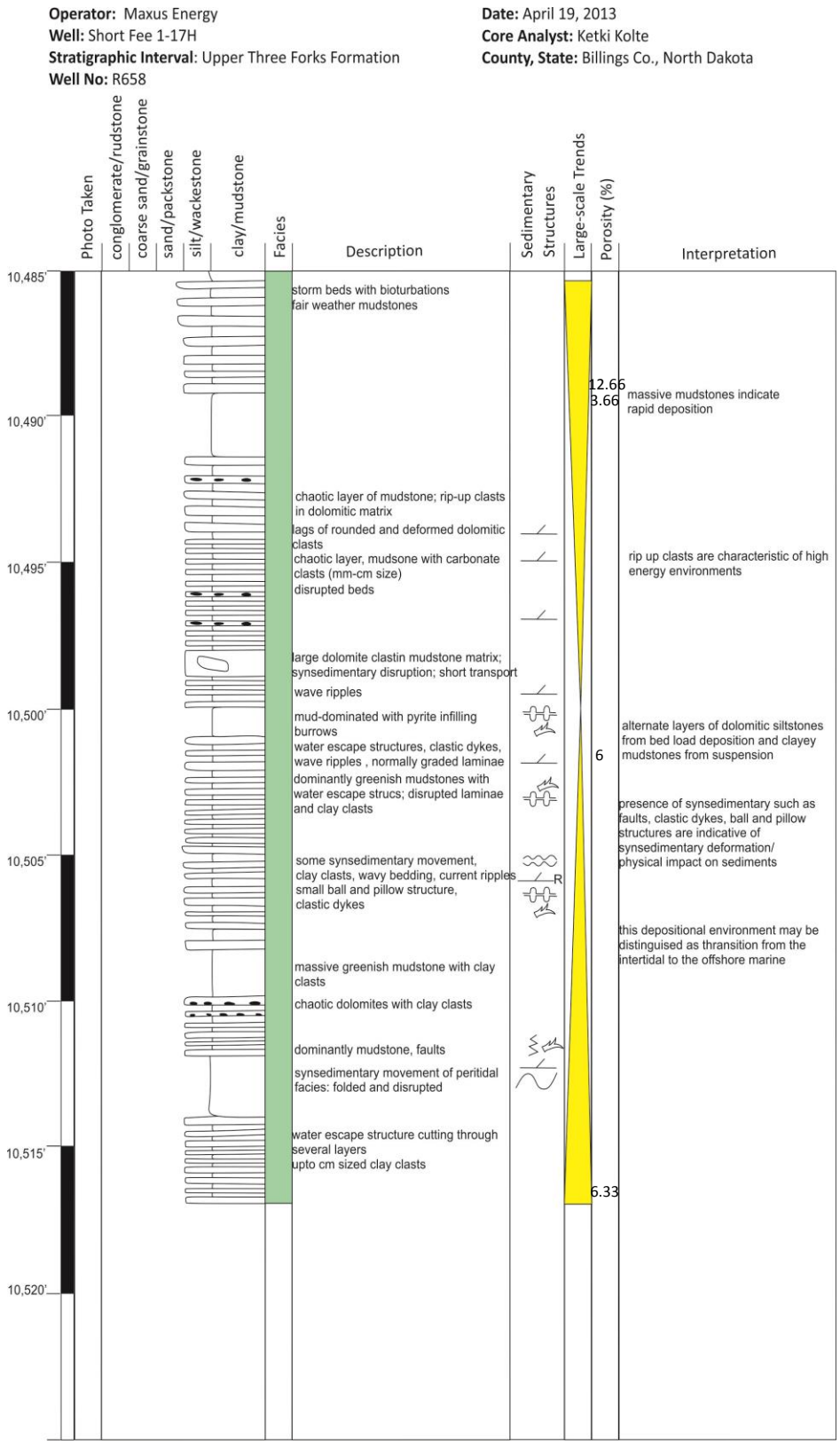

Figure 26: Stratigraphic description of Core #R658